Wetting films on chemically heterogeneous substrates

C. Bauer and S. Dietrich
Fachbereich Physik, Bergische Universität Wuppertal, D-42097 Wuppertal, Germany
(Received 11 June 1999)

Based on a microscopic density functional theory, we investigate the morphology of thin liquidlike wetting films adsorbed on substrates endowed with well-defined chemical heterogeneities. As paradigmatic cases we focus on a single chemical step and on a single stripe. In view of applications in microfluidics, the accuracy of guiding liquids by chemical microchannels is discussed. Finally we give a general prescription of how to investigate theoretically the wetting properties of substrates with arbitrary chemical structures.
[S1063-651X(99)07011-7]

PACS number(s): 68.45.Gd, 68.10.−m, 82.65.Dp

I. INTRODUCTION

A large variety of experimental techniques has emerged which allows one to endow solid substrates with stable, persistent, and well-defined lateral patterns of a geometrical or a chemical nature, or a combination thereof [1–6]. The spatial extension of these regular structures ranges from the μm scale down to nm. A major part of the application potential of such manmade surfaces is based on their exposure to fluids and their ability to imprint permanent, well-defined structures on adjacent soft matter encompassing simple anorganic and organic liquids as well as complex fluids such as polymer solutions or colloidal suspensions (see, e.g., Ref. [7]).

Here we are interested in planar, chemically structured surfaces. Recent experiments have explored the wetting and adsorption properties of fluids and polymer solutions on such heterogeneous surfaces [8–15]; some studies even have demonstrated the feasibility to control the growth of biological systems by attaching them to structured surfaces [16,17], and to recognize biological molecules, e.g., proteins, selectively by bringing them into contact with nanostructured surfaces [18,19]. In the context of microfluidics [20,21], one is interested in guiding small quantities of valuable liquids to designated sites where they can either be analyzed or undergo chemical reactions. This transportation problem can be solved by using microgrooves or microchannels. Alternatively, liquids can be guided along chemical lanes on flat substrates. Such an integrated network can be used to build chemical chips and tiny chemical factories (see, e.g., Ref. [22]). This development has been greatly facilitated by the emergence of microcontact printing [23–26] as an important technique to cover solid substrates with designed chemical patterns. With this technique one can create surface patterns which consist of regular monolayer patches composed of different chemical species. These patterns are anchored at a homogeneous and flat substrate such that the resulting decorated surface remains flat on a molecular scale. Such a patchwork of, e.g., hydrophilic and hydrophobic areas with lateral extensions in the submicrometer range can be designed with high precision, and turns out to be rather robust.

In view of the desired miniaturization of such structures a question arises of the extent to which thermal fluctuations limit the ability to keep adsorbed liquids with high lateral precision on the designated chemical patterns without spilling. Moreover, one would like to know which chemical and structural architecture of the manmade surface is favorable for miniaturization. This requires decoding the relation between the structural properties of the highly inhomogeneous liquids and the molecular interaction potentials of the fluid particles and of the various, specifically arranged substrate particles.

We address some of these issues for the case of thermal equilibrium by suitable tools of statistical mechanics. Different theoretical models have already been applied to study various basic properties of adsorption of liquids on structured substrates. Exact virial theorems and compressibility sum rules, as they can be formulated for fluids in contact with homogeneous walls, have also been derived for heterogeneous substrates [27]. In this context phenomenological interface displacement and square-gradient models [14,28–34], as well as lattice gas models [35–37], highlight the general behavior of liquidlike wetting layers and their singular properties at surface or morphological phase transitions. More sophisticated theories such as density functional theories [38–43] and computer simulations [11,44–47] have the potential to investigate in detail the role of microscopic interactions, and to resolve the fine structures of the fluids under consideration on a molecular scale. Whereas the former theories are based on severe simplifications and focus on idealized systems on a macroscopic scale (i.e., μm and larger), the latter require high computational efforts such that only rather small systems like pores and slits can be studied. Our present analysis is supposed to provide a link between these two approaches in that it keeps track of the microscopic molecular interactions between the various constituents but leaves out fine structures on a molecular scale. This allows us to investigate liquidlike structures on a mesoscopic scale commensurate with the actual experimental system sizes. As basic ingredients for the molecular interactions we adopt Lennard-Jones, i.e., long-ranged, interaction potentials. These potentials are not only applicable for rare gases, but also resemble reliable effective potentials for molecules like small alkanes or alcohols [48].

In order to provide the information and terminology required for the subsequent considerations in Sec. II, we recall some basic results for the wetting of flat and homogeneous substrates [49,50], and extend them to the case of homogeneous substrates covered by a laterally homogeneous over-

layer. In Sec. III we present the theoretical basis for our analysis of the wetting of chemically structured substrates, from which we derive many analytical and numerical results in Secs. IV and V, respectively. These results extend and complete earlier studies which also focused on the mesoscopic structure of liquidlike layers on heterogeneous substrates [38,51]. Our analysis is carried out within mean field theory without taking into account capillary wavelike fluctuations and the strong fluctuations arising near critical points of the fluids. We focus our analysis on three paradigmatic chemical surface structures: a chemical step generated by two adjacent quarter spaces filled with different materials, a chemical step generated by two different adjacent surface layers covering a homogeneous substrate, and a chemical stripe generated by a slab of different material immersed in an otherwise homogeneous substrate orthogonal to the common flat surface. Finally, in Sec. VI we extend our approach to arbitrary chemically structured substrates, and summarize our results in Sec. VII. Technical details of the substrate potentials and of the density functional description are presented in Appendixes A and B, respectively.

II. WETTING OF LATERALLY HOMOGENEOUS SUBSTRATES

A. Density functional theory

Our theoretical analysis is based on the following simple [52] but nonetheless successful [50] density functional theory for a spatially inhomogeneous number density $\rho(\mathbf{r})$ of fluid particles:

$$\Omega([\rho(\mathbf{r})];T,\mu)=\int_\Lambda d^3r\ f_{\mathrm{HS}}(\rho(\mathbf{r}),T) + \int_\Lambda d^3r[V(\mathbf{r})-\mu]\rho(\mathbf{r}) + \frac{1}{2}\int_\Lambda d^3r\int_\Lambda d^3r'\ \tilde{w}(|\mathbf{r}-\mathbf{r}'|)\rho(\mathbf{r})\rho(\mathbf{r}'). \tag{2.1}$$

The minimum of $\Omega[\rho(\mathbf{r})]$ with respect to $\rho(\mathbf{r})$ yields the grand canonical free energy of the fluid corresponding to a prescribed temperature T and chemical potential μ. $V(\mathbf{r})$ denotes the substrate potential, and $\tilde{w}(\mathbf{r})$ is the attractive part of the fluid interparticle potential. Λ is the volume occupied by the fluid particles. f_{HS} is the free energy density of a hard-sphere reference fluid. This contribution takes into account the repulsive part of the fluid interparticle potential within a local density approximation which neglects short-ranged particle-particle correlations. These correlations become important in the close vicinity of the substrate surface. Nonetheless Eq. (2.1) has turned out to provide a very useful description of wetting phenomena in the case when the adsorbed liquidlike films are much thicker than the diameter σ_f of the fluid particles.

The fluid particles are assumed to interact via a Lennard-Jones potential

$$\phi_f(r)=4\epsilon_f\left[\left(\frac{\sigma_f}{r}\right)^{12}-\left(\frac{\sigma_f}{r}\right)^{6}\right]. \tag{2.2}$$

We apply the Weeks-Chandler-Andersen (WCA) procedure [53] to split up this interaction into an attractive part $\phi_{\mathrm{att}}(r)$ and a repulsive part $\phi_{\mathrm{rep}}(r)$. The latter gives rise to an effective, temperature dependent, hard sphere diameter

$$d(T)=\int_0^{2^{1/6}\sigma_f}dr\left\{1-\exp\left(-\frac{\phi_{\mathrm{rep}}(r)}{k_BT}\right)\right\}, \tag{2.3}$$

which is inserted into the Carnahan-Starling approximation for the free energy density of the hard-sphere fluid [54],

$$f_{\mathrm{HS}}(\rho,T)=k_BT\rho\left(\ln(\rho\lambda^3)-1+\frac{4\eta-3\eta^2}{(1-\eta)^2}\right), \tag{2.4}$$

where $\eta=(\pi/6)\rho[d(T)]^3$ is the dimensionless packing fraction and λ is the thermal de Broglie wavelength.

The attractive part of the interaction $\phi_{\mathrm{att}}(r)$ is approximated by

$$\tilde{w}(r)=\frac{4w_0\sigma_f^3}{\pi^2}(r^2+\sigma_f^2)^{-3}, \tag{2.5}$$

with

$$w_0=\int_{\mathbb{R}^3}d^3r\ \tilde{w}(r)=\int_{\mathbb{R}^3}d^3r\ \phi_{\mathrm{att}}(r)=-\frac{32}{9}\sqrt{2}\pi\epsilon_f\sigma_f^3. \tag{2.6}$$

Although Eq. (2.5) does not strictly implement the WCA procedure corresponding to Eq. (2.2), it resembles it closely, and offers the valuable advantage of reduced computational efforts because the form of $\tilde{w}(r)$ allows one to carry out certain integrations over $\tilde{w}(r)$ analytically. For large particle separations r, one has $\tilde{w}(r\to\infty)\sim r^{-6}$; the amplitude is chosen such that the integrated strength equals that of the attractive contribution ϕ_{att} obtained by the strict application of the WCA procedure. The third integral in Eq. (2.1) takes into account the attractive fluid interparticle interaction within mean field theory based on Eq. (2.5).

B. Bulk phases

In a bulk system the particle density ρ_γ (where $\gamma=l$ and $\gamma=g$ denote the liquid and vapor phase, respectively) is spatially constant, leading to [see Eq. (2.1)]

$$\Omega_b(\rho_\gamma,T,\mu)=f_{\mathrm{HS}}(\rho_\gamma,T)+\frac{1}{2}w_0\rho_\gamma^2-\mu\rho_\gamma \tag{2.7}$$

for the grand canonical free energy density of a bulk fluid. Minimization of Ω_b with respect to ρ_γ yields the equilibrium densities. The conditions for liquid-vapor phase coexistence $\mu=\mu_0(T)$ are

$$\left.\frac{\partial\Omega_b}{\partial\rho}\right|_{\rho=\rho_g}=\left.\frac{\partial\Omega_b}{\partial\rho}\right|_{\rho=\rho_l}=0 \quad\text{and}\quad \Omega_b(\rho_g)=\Omega_b(\rho_l). \tag{2.8}$$

Off coexistence, i.e., for $\mu\neq\mu_0$, only the liquid or vapor phase is stable. In this case the density of the metastable phase corresponds to the second local minimum of Ω_b.

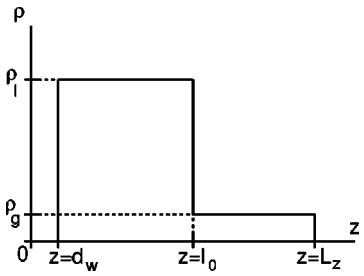

FIG. 1. Sharp-kink approximation for the particle density distribution. At the position $z=l_0$ of the liquid-vapor interface there is a steplike variation of the particle density between the bulk liquid (ρ_l) and the bulk vapor density (ρ_g). At $z=L_z$ the density is truncated in order to facilitate the thermodynamic limit. Due to the repulsion between the fluid and the substrate particles the particle density vanishes for $z<d_w$, giving rise to an excluded volume.

C. Wetting of laterally homogeneous substrates

Here we recall some basic results for wetting phenomena (for reviews see, e.g., Refs. [50,55–58]) as they follow from Eq. (2.1) for a homogeneous substrate within the so-called sharp-kink approximation (see Fig. 1 and Ref. [50]). This allows us to formulate our corresponding findings for substrates which are heterogeneous either in the direction normal to the surface or in lateral directions.

In the following we consider a flat substrate located in the half space $w=\{\mathbf{r}\in\mathbb{R}^3|z\leqslant 0\}$. The substrate is either homogeneous or composed of a homogeneous part $w_H=\{\mathbf{r}\in\mathbb{R}^3|z<-dg_z\}$ covered by a homogeneous surface layer $w_S=\{\mathbf{r}\in\mathbb{R}^3|-dg_z\leqslant z\leqslant 0\}$ of different chemical species. It consists of particles located on an orthorhombic lattice with lattice constants g_i in the i direction ($i=x,y,z$). For reasons of simplicity the lattice constant g_z is assumed to be constant throughout the whole substrate. The surface layer consists of $n=d+1$ monolayers, with the uppermost and lowest monolayers located at $z=0$ and $z=-dg_z$, respectively. The theoretical description [Eq. (2.1)] is identical for both substrate types; it only differs with respect to the considered substrate potential $V(z)$. The substrate acts as an inert spectator phase. The interaction potential between a fluid particle and an individual substrate particle is also taken to be of Lennard-Jones type,

$$\phi_{H,S}(r)=4\epsilon_{H,S}\left[\left(\frac{\sigma_{H,S}}{r}\right)^{12}-\left(\frac{\sigma_{H,S}}{r}\right)^{6}\right] \tag{2.9}$$

where H and S denote the molecules in w_H and w_S, respectively. The substrate potential $V(\mathbf{r})\equiv V(z)=V_{\mathrm{att}}(z)+V_{\mathrm{rep}}(z)$ follows as a laterally averaged pairwise sum of $\phi_{H,S}$ over all substrate particles, resulting in

$$\begin{aligned}V_{\mathrm{att}}(z)&=-\frac{u_3^H}{(z+(d+1)g_z)^3}-\frac{u_4^H}{(z+(d+1)g_z)^4}\\&\quad-u_3^S\left(\frac{1}{z^3}-\frac{1}{(z+dg_z)^3}\right)-u_4^S\left(\frac{1}{z^4}+\frac{1}{(z+dg_z)^4}\right)\\&\quad+\mathcal{O}(z^{-5})\\&=-\frac{u_3^H}{z^3}-\frac{2(d+1)u_4^S-(2d+1)u_4^H}{z^4}\\&\quad+\mathcal{O}(z^{-5}),\quad z\gg dg_z\end{aligned} \tag{2.10}$$

for the attractive potential. In Eq. (2.10) we have used the relations $u_4^{H,S}=\frac{3}{2}g_z u_3^{H,S}$. Moreover, the coefficients can be expressed in terms of the parameters $\epsilon_{H,S}$ and $\sigma_{H,S}$ of the molecular interactions and the lattice spacing g_z. The repulsive contribution is

$$\begin{aligned}V_{\mathrm{rep}}(z)&=\frac{u_9^H}{(z+(d+1)g_z)^9}+\frac{u_{10}^H}{(z+(d+1)g_z)^{10}}\\&\quad+u_9^S\left(\frac{1}{z^9}-\frac{1}{(z+dg_z)^9}\right)+u_{10}^S\left(\frac{1}{z^{10}}+\frac{1}{(z+dg_z)^{10}}\right)\\&\quad+\mathcal{O}(z^{-11})\\&=\frac{u_9^H}{z^9}+\mathcal{O}(z^{-10}),\quad z\gg dg_z.\end{aligned} \tag{2.11}$$

In the case of a homogeneous substrate, $u_i^S=u_i^H=u_i$, $V(z)$ reduces to

$$V(z)=-\sum_{j\geqslant 3}\frac{u_j}{z^j}. \tag{2.12}$$

The limit $d\to\infty$ corresponds to a homogeneous substrate composed of the chemical species of the surface layer.

For the above model the full minimization of the functional in Eq. (2.1) with respect to the spatially inhomogeneous, smooth density $\rho(z)$ can be carried out only numerically. However, it has turned out that the minimization restricted to the subspace of piecewise constant density profiles provides a surprisingly accurate *analytic* account of the corresponding effective interface potential [59,60]. Within this so-called sharp-kink approximation (Fig. 1),

$$\hat{\rho}(z)=\Theta(z-d_w)[\Theta(l-z)\rho_l+\Theta(z-l)\rho_g], \tag{2.13}$$

ρ_l and ρ_g are the number densities of the bulk liquid and vapor phase, respectively (see Sec. II B). For $\mu<\mu_0$, ρ_g is taken to be the actual vapor density off coexistence, and ρ_l is the density of the metastable liquid phase. Θ denotes the Heaviside step function, and l is the thickness of the adsorbed liquidlike wetting layer, i.e., $z=l$ is the position of the emerging liquid-vapor interface. In terms of the actual smooth density distribution $\rho(z)$ the position of the interface can be defined by, e.g., $\rho(z=l)=\frac{1}{2}(\rho_l+\rho_g)$. The length d_w takes into account the excluded volume for the centers of the fluid particles due to the repulsive part of the substrate potential. We assume that $d_w=\frac{1}{2}(\sigma_w+\sigma_f)$. The insertion of Eq. (2.13) into Eq. (2.1) yields

$$\begin{aligned}&\Omega([\hat{\rho}(z)];T,\mu;[\hat{w}],[V])\\&\quad=\Lambda\Omega_b(\rho_b;T,\mu)+A\Omega_s([\hat{\rho}(z)];T,\mu;[\tilde{w}],[V]),\end{aligned} \tag{2.14}$$

i.e., a decomposition of the grand canonical functional into bulk and surface contributions. Λ is the volume occupied by fluid particles. In the thermodynamic limit this is the half space $\{\mathbf{r}=(\mathbf{r}_\parallel,z)\in\mathbb{R}^3|z>0\}$. A is the area of the substrate surface. Ω_b is given by Eq. (2.7) whereas Ω_s yields the so-called effective interface potential $\Omega_s(l)$

$$\Omega_s([\hat{\rho}(z)])=\Omega_s(l)=\Delta\Omega_b l+\sigma_{wl}+\sigma_{lg}+\omega(l). \tag{2.15}$$

The first term in Eq. (2.15) measures the cost in free energy for forming a liquidlike wetting layer of thickness l if in the bulk the vapor is the stable phase. One has $\Delta\Omega_b=\Delta\rho\Delta\mu+\mathcal{O}((\Delta\mu)^2)$ where $\Delta\mu=\mu_0-\mu$. With

$$t(z)=\int_z^\infty dz'\int_{\mathbb{R}^2}d^2r_\parallel\,\tilde{w}(\sqrt{r_\parallel^2+z'^2}) \tag{2.16}$$

as the potential of a fluid particle interacting with a half space filled with the same fluid particles, within the above sharp-kink approximation, for the substrate-liquid surface tension, one has

$$\sigma_{wl}=-\frac{1}{2}\rho_l^2\int_0^\infty dz\;t(z)+\rho_l\int_{d_w}^\infty dz\;V(z)-d_w\Omega_b^{(l)} \tag{2.17}$$

and

$$\sigma_{lg}=-\frac{1}{2}(\Delta\rho)^2\int_0^\infty dz\;t(z) \tag{2.18}$$

for the liquid-vapor surface tension. The l-dependent part $\omega(l)$ of the effective interface potential is given by

$$\omega(l)=\Delta\rho\left\{\rho_l\int_{l-d_w}^\infty dz\;t(z)-\int_l^\infty dz\;V(z)\right\}. \tag{2.19}$$

Minimization of the interfacial free energy $\Omega_s(l)$ with respect to l yields the equilibrium film thickness l_0 and the substrate-vapor surface tension $\sigma_{wg}=\min_{\{l\}}\Omega_s(l)=\Omega_s(l_0)$. From Young's equation, for the contact angle one obtains $\cos(\theta)=(\sigma_{wg}-\sigma_{wl})/\sigma_{lg}=1+\omega(l_0)/\sigma_{lg}$, which is thermodynamically well defined only at two-phase coexistence $\Delta\mu=0$.

From Eqs. (2.5) and (2.16), one has $t(z)=-\Sigma_{j\geqslant 3}t_j z^{-j}$, and therefore

$$\omega(l)=\sum_{j\geqslant 2}\frac{a_j}{l^j}. \tag{2.20}$$

[Here we do not consider terms $\sim l^{-5}\ln l$ generated by van der Waals tails in the density profiles [60(c)] which are not captured by the ansatz in Eq. (2.13).] The coefficients of the leading terms are $a_2=(\Delta\rho/2)(u_3^H-t_3\rho_l)$, which is known as the Hamaker constant, and $a_3=(\Delta\rho/3)(2(d+1)u_4^S-(2d+1)u_4^H-(t_4+3t_3d_w)\rho_l)$; for a homogeneous substrate with $u_j^S=u_j^H=u_j$ one has $a_3=(\Delta\rho/3)(u_4-(t_4+3t_3d_w)\rho_l)$. We note that the Hamaker constant for a homogeneous substrate covered by a homogeneous surface layer does not depend on the properties of the surface layer but all subdominant terms do.

The substrate is said to be *completely wet* by the liquid phase if, at coexistence $\Delta\mu=0$, l_0 is infinite. Since $\omega(l_0=\infty)=0$ one has $\sigma_{wg}=\sigma_{wl}+\sigma_{lg}$ and $\theta=0$ for completely wet substrates and $\sigma_{wg}<\sigma_{wl}+\sigma_{lg}$ and $\theta>0$ for partially wet substrates. If at $T=T_w$ the thickness $l_0(T,\mu=\mu_0)$ jumps from a finite value for $T<T_w$ to $l_0=\infty$ for $T>T_w$, the system undergoes a *first order wetting transition*. If the film thickness grows continuously upon approaching the wetting temperature, i.e., $l(T\to T_w,\mu=\mu_0)\to\infty$, the system exhibits a *critical wetting transition*. The necessary condition for critical wetting is that $a_2(T)$ changes sign at T_w from $a_2(T<T_w)<0$ to $a_2(T>T_w)>0$ and $a_3(T=T_w)>0$, i.e., $u_4-(t_4+3t_3d_w)\rho_l(T_w)>0$. The critical wetting transition temperature is given implicitly by $u_3^H=t_3\rho_l(T_w)$, or, equivalently, $u_3=t_3\rho_l(T_w)$ for a homogeneous substrate. Even with an additional surface layer, which modifies the substrate potential in the vicinity of the substrate surface, the transition temperature of a critical wetting transition is determined only by the properties of the underlying homogeneous substrate w_H. This implies that two substrates which differ only with respect to their overlayers have the same wetting transition temperature if the wetting transition is continuous. From the above formulas one can infer that the occurrence of a critical wetting transition on a planar and homogeneous substrate hinges on the subdominant contribution $\sim z^{-4}$ in the asymptotic expansion of $V(z)$ for large z because for the attractive fluid-fluid interaction as given by Eq. (2.5) $t_4=0$ and $t_3=-(2/3\pi)w_0\sigma_f^3>0$. It is possible to fulfill the necessary condition $a_3(T_w)>0$ for critical wetting by choosing an appropriate surface layer. In the case of critical wetting the film thickness diverges as $l_0(T\nearrow T_w)=-3a_3/2a_2\sim(T_w-T)^{-1}$. Irrespective of the order of the wetting transition, upon approaching coexistence along a complete wetting isotherm one has $l_0(T>T_w,\Delta\mu\searrow 0)=(2a_2/\Delta\Omega_b)^{1/3}\sim(\Delta\mu)^{-1/3}$. For $T>T_w$ the Hamaker constant a_2 is always positive. The leading divergence of l_0 for a complete wetting transition is independent of any different surface layer covering the substrate.

III. MODELS FOR WETTING OF STRUCTURED SUBSTRATES

A. Simple chemical step

As a basic element for more complicated structures, we first analyze the wetting properties of a substrate which exhibits a single, simple chemical step (SCS), i.e., a flat substrate composed of two adjacent quarter spaces filled with different chemical species (see Fig. 2, with $n=\infty$). The substrate particles occupy the half space $w=\{\mathbf{r}\in\mathbb{R}^3|z\leqslant 0\}$ and the heterogeneity defines the position $x=0$. The system is translationally invariant along the y direction. The substrate and the fluid particles interact via Lennard-Jones potentials

$$\phi_\pm(r)=4\epsilon_\pm\left[\left(\frac{\sigma_\pm}{r}\right)^{12}-\left(\frac{\sigma_\pm}{r}\right)^{6}\right], \tag{3.1}$$

where the ''+'' and ''−'' signs refer to substrate particles located in the quarter spaces $w_+=\{\mathbf{r}\in\mathbb{R}^3|x>0\wedge z\leqslant 0\}$ and $w_-=\{\mathbf{r}\in\mathbb{R}^3|x<0\wedge z\leqslant 0\}$, respectively. The substrate potential $V(x,z)=V_{\rm att}(x,z)+V_{\rm rep}(x,z)$, as obtained by a pair-

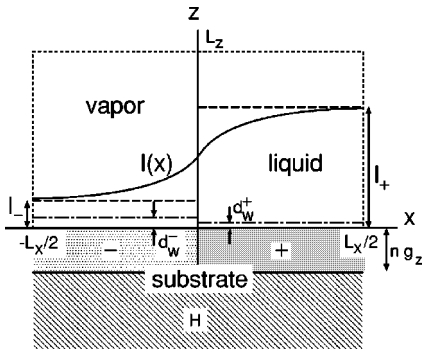

FIG. 2. Morphology $l(x)$ of a liquidlike film which covers a flat, heterogeneous substrate [layer chemical step (LCS)]. The substrate surface is located at $z=0$. In general the substrate consists of a homogeneous part (denoted as H) which is covered by two adjacent, semi-infinite surface layers composed of different chemical species ($+$ and $-$) which form a sharp chemical boundary at $x=0$. The surface layer consists of $n=d+1$ molecular monolayers with a lattice spacing g_z in the z direction. The limit $n\to\infty$ corresponds to a substrate which exhibits a single simple chemical step (SCS). $l_\mp = l(x\to\mp\infty)$ are the equilibrium film thicknesses of the corresponding substrates composed of H plus a laterally homogeneous surface layer ($+$ or $-$). We assume that H covered by a $+$ layer is the stronger substrate favoring the adsorption of thicker liquidlike films, i.e., $l_+ > l_-$. The two substrate halves are characterized by different excluded volumes $d_w^\pm$ (dash-dotted lines). The system is translationally invariant in the y direction and truncated at $z=L_z$ and $x=\mp L_x/2$ in order to facilitate the proper thermodynamic limit. The long-dashed line corresponds to the sharp-kink approximation for the *lateral* profile.

wise summation over all substrate particles, is given by Eqs. (A2) and (A3) in Appendix A. In the limit $|x|\to\infty$, $V(x,z)$ asymptotically approaches the substrate potential of the respective homogeneous substrate:

$$V(x\to\pm\infty,z) = -\frac{u_3^\pm}{z^3} - \frac{u_4^\pm}{z^4} + \frac{u_9^\pm}{z^9} + \frac{u_3^+ - u_3^-}{2x^3} + \mathcal{O}(x^{-4})$$
$$= V_\pm(z) + \frac{u_3^+ - u_3^-}{2x^3} + \mathcal{O}(x^{-4}), \tag{3.2}$$

where the coefficients of the subdominant terms omitted here depend on z. Thus the adsorbed liquidlike wetting film exhibits the asymptotic thicknesses l_+ for $x\to\infty$ and l_- for $x\to-\infty$ which are determined by the properties of the homogeneous substrates ''+'' and ''−,'' respectively. In general one has to take into consideration two different wetting temperatures T_w^+ and T_w^-, one for each of the two semi-infinite, homogeneous substrates.

With the substrate potential $V(x,z)$ given, in principle the functional in Eq. (2.1) can be minimized with respect to the full density distribution $\rho(x,z)$. However, this can only be done numerically, and requires a huge computational effort. Therefore, we focus on low temperatures, which allows us to restrict the minimization to steplike profiles

$$\hat\rho(x,z) = [\Theta(-x)\Theta(z-d_w^-) + \Theta(x)\Theta(z-d_w^+)]$$
$$\times[\rho_l\Theta(l(x)-z) + \rho_g\Theta(z-l(x))]. \tag{3.3}$$

The quantities $d_w^\pm = \frac{1}{2}(\sigma_\pm + \sigma_f)$ take into account the different excluded volumes in the vicinity of the substrate surface. Because of the rapid decay of the repulsive forces, d_w is taken to vary steplike at $x=0$ between d_w^+ and d_w^-. The approximation used in Eq. (3.3) does not capture the fluid density oscillations very close to the substrate surface. However, these fine structures of the particle density are expected to have only small effects if the liquidlike wetting films are rather thick, as is the case in the vicinity of a critical or a complete wetting transition. The sharp-kink approximation yields an exact prediction for the transition temperature T_w of a critical wetting transition which remains unchanged if more sophisticated models are applied [59]. Although within the sharp-kink approximation the predicted thickness of adsorbed liquidlike wetting layers is not quantitatively accurate, this approach is expected to capture the essential features of the wetting phenomena as considered on the present mesoscopic scale.

The grand canonical free energy functional—which via Eq. (3.3) is a functional of the function $l(x)$ that describes the local position of the liquid-vapor interface—can be systematically decomposed into bulk, surface, and line contributions:

$$\Omega([\hat\rho(x,z)];T,\mu;[\tilde w],[V]) = \Lambda\Omega_b(\rho_g,T,\mu)$$
$$+ A\Omega_s(l_\pm;T,\mu;[\tilde w],[V])$$
$$+ L_y\Omega_l([l(x)];T,\mu;[\tilde w],[V]). \tag{3.4}$$

The explicit expressions for these contributions are given in Appendix B. In Eq. (3.4), $\Lambda = L_x L_y L_z$ is the volume filled with fluid particles, $A = L_x L_y$ is the surface area of the substrate surface, and L_y is the linear extension of the chemical step. Ω_b, given by Eq. (2.7), is the bulk free energy density corresponding to the stable bulk vapor phase. The surface contribution

$$\Omega_s(l_\pm) = \frac{1}{2}[\Omega_s^+(l_+) + \Omega_s^-(l_-)] \tag{3.5}$$

is the arithmetic mean of the surface free energy densities corresponding to the substrates w_+ and w_- covered by liquidlike films of thickness l_+ and l_- which are exposed to the potentials $V_+(z)$ and $V_-(z)$, respectively [see Eq. (2.15)]. $l_\pm$ minimizes the corresponding equation (2.15), with ρ_g and ρ_l as the bulk vapor phase and the metastable bulk liquid phase, respectively.

The line contribution Ω_l is due to the substrate heterogeneity, and reads

$$\Omega_l[l(x)] = \tau(d_w^\pm, l_\pm) + \tilde\omega[l(x)]. \tag{3.6}$$

The expression $\tau(d_w^\pm, l_\pm)$ does not depend on the profile $l(x)$. Minimization of the *nonlocal* functional $\tilde\omega[l(x)]$ [which is given in Eq. (B4)] yields the equilibrium liquid-vapor interface profile $\overline{l}(x)$ and the line tension

$$\tau(T,\mu) = \min_{\{l(x)\}} \Omega_l[l(x)] = \Omega_l[\overline{l}(x)]. \tag{3.7}$$

A gradient expansion of $\tilde{\omega}[l(x)]$ in leading order leads to the *local* functional $\tilde{\omega}_{\mathrm{loc}}[l(x)]$ [see Eq. (B9)] that provides a prescription of how to express the functional expressions given by a simple, phenomenological interface displacement model in terms of the microscopic parameters of the underlying molecular interactions.

The Euler-Lagrange equation (ELE) following from the functional derivative of the nonlocal functional $\tilde{\omega}[l(x)]$ is

$$\left.\frac{\delta\Omega_l[l(x)]}{\delta l(x)}\right|_{l=\bar{l}} = \left.\frac{\delta\tilde{\omega}[l(x)]}{\delta l(x)}\right|_{l=\bar{l}}$$
$$= \Delta\Omega_b - \Delta\rho[\rho_l t(\bar{l}(x)-d_w^+) - V(x,\bar{l}(x))]$$
$$+ I(x,\bar{l}(x)) + \Delta\rho\rho_l\{\bar{t}(x,\bar{l}(x)-d_w^+)$$
$$- \bar{t}(x,\bar{l}(x)-d_w^-)\} = 0, \tag{3.8}$$

with $\bar{t}(x,z)$ given by Eq. (B7) and

$$I(x,l(x)) \equiv (\Delta\rho)^2 \int_{-\infty}^{\infty} dx' \int_0^{l(x')-l(x)} dz'\ \bar{w}(x-x',z'), \tag{3.9}$$

where $\bar{w}(x,z)$ is given by Eq. (B8). The ELE is a nonlocal integral equation for the function $\bar{l}(x)$. Within the local theory the double integral in Eq. (3.9) is replaced by a differential expression leading to

$$I_{\mathrm{loc}}(l(x)) \equiv \frac{\sigma_{lg} l''(x)}{[1+(l'(x))^2]^{3/2}}$$
$$= \Delta\Omega_b - \Delta\rho[\rho_l t(\bar{l}(x)-d_w^+) - V(x,\bar{l}(x))]$$
$$+ \Delta\rho\rho_l\{\bar{t}(x,\bar{l}(x)-d_w^+) - \bar{t}(x,\bar{l}(x)-d_w^-)\}. \tag{3.10}$$

Equation (3.10) is often referred to as ''augmented Young equation'' [61].

B. Chemical step within a surface layer

The analysis in Sec. III A requires that the substrate be composed of two adjacent halves which themselves are homogeneous along both the x and y directions. However, it is not necessary that the substrate halves are chemically homogeneous in the z direction.

This allows us to consider within the same formalism a homogeneous substrate w_H covered by a surface layer which itself is composed of two adjacent homogeneous layers $w_{S,\pm} = \{\mathbf{r} \in \mathbb{R}^3 | x \gtrless 0 \wedge -dg_z < z < 0\}$ of different chemical species. In the following we refer to this type of substrate as a layer chemical step (LCS). The two halves of the layer meet at $x=0$ (see Fig. 2). Both surface layers consist of $n = d+1$ monolayers, with the uppermost and the lowest monolayer located at $z=0$ and $z=-dg_z$, respectively. This model mimics rather closely the kind of substrate inhomogeneities generated by, e.g., microcontact printing (see Sec. I). The expression for the substrate potential $V(x,z)$ of this system is rather complicated [see Eqs. (A4) and (A5)]. As mentioned in Sec. II C, the leading contribution to the attractive substrate potential is only determined by the underlying homogeneous substrate w_H. Thus when both substrate halves undergo a critical wetting transition there is only a single common wetting temperature T_w for the whole substrate because the Hamaker constant is only determined by w_H.

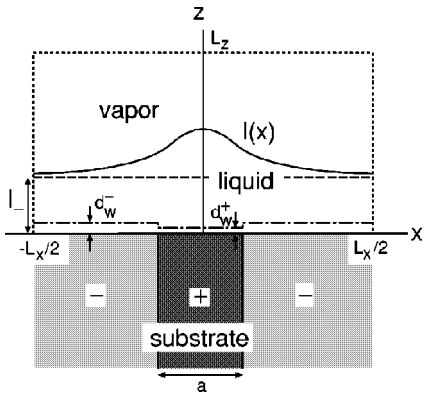

FIG. 3. Morphology of a liquidlike film which covers a flat substrate exhibiting a ''chemical stripe'' (CST). A slab consisting of chemical species denoted by + is immersed in a homogeneous − substrate. Thus in top view a chemical stripe with two sharp chemical steps is formed. The slab extends from $x=-a/2$ to $x=a/2$, i.e., the stripe width is a. $l_-=l(|x|\to\infty)$ is the equilibrium thickness of the liquidlike wetting film corresponding to the homogeneous substrate composed of ''−'' particles. In contrast to the SCS and LCS (compare Fig. 2), here both cases $l_+ > l_-$ and $l_+ < l_-$—where l_+ corresponds to the film thickness on the homogeneous + substrate—have to be considered. The slab and the embedding substrate exhibit different excluded volumes $d_w^{\pm}$. The system is translationally invariant in the y direction and truncated at $z=L_z$ and $x=\mp L_x/2$ in order to facilitate the proper thermodynamic limit.

Far from the heterogeneity, for fixed z, the potential $V(x,z)$ asymptotically approaches the substrate potentials $V_{\pm}(z)$ of the two semi-infinite, laterally homogeneous substrate halves covered by a surface layer via

$$V(x\to\pm\infty,z) = V_{\pm}(z) + \mathrm{sgn}(x)\frac{3(d+1)(u_4^+-u_4^-)}{8}\frac{1}{x^4}$$
$$+ \mathcal{O}(x^{-5}). \tag{3.11}$$

Again the coefficients of the subdominant terms omitted here depend on z. From Eq. (3.11) it follows that the wetting layer thickness $l(x)$ asymptotically approaches the constant values $l_{\pm}$ corresponding to the respective decorated substrate.

C. Chemical stripe

As a third system we consider a substrate exhibiting a chemical stripe (CST). The stripe is realized by insertion of a slab $w_{\mathrm{st}} = \{\mathbf{r} \in \mathbb{R}^3 | |x| < a/2 \wedge z \leqslant 0\}$ of different chemical species + into an otherwise homogeneous substrate $w = \{\mathbf{r} \in \mathbb{R}^3 | z \leqslant 0\}$ composed of particles denoted as −, such that in the top view a chemical stripe is formed (see Fig. 3). The system is again translationally invariant in the y direction.

The substrate potential $V(-x,z)=V(x,z)$ is given by Eqs. (A6) and (A7). For z fixed in the limit of large $|x|$, one has

$$V(|x|\to\infty,z)=-\frac{u_3^-}{z^3}-\frac{u_4^-}{z^4}+\frac{u_9^-}{z^9}-\frac{a}{g_x}\,\frac{u_{4,x}^+-u_{4,x}^-}{x^4}+\mathcal{O}(x^{-5}) \tag{3.12}$$

(where again only the coefficients of the subdominant terms depend on z), implying that the equilibrium liquid-vapor interface is also symmetric with respect to $x=0$, i.e., $l(-x)=l(x)$, and that it asymptotically approaches the constant value l_- for $|x|\to\infty$ determined by the properties of the homogeneous, flat substrate w. For a wide stripe width one has

$$V(x,z)=-\frac{u_3^+}{z^3}-\frac{u_4^+}{z^4}+\frac{u_9^+}{z^9}+\mathcal{O}(a^{-3}),$$

$$a\gg g_x \quad \text{and} \quad |x|\ll a/2, \tag{3.13}$$

so that for small $|x|$ the profile $l(x)$ is close to the film thickness l_+ of a liquidlike film on the homogeneous and planar + substrate.

The sharp-kink density profile used for the analysis of the CST is

$$\hat{\rho}(x,z)=\left\{\Theta\left(|x|-\frac{a}{2}\right)\Theta(z-d_w^-)+\Theta\left(\frac{a}{2}-|x|\right)\Theta(z-d_w^+)\right\}\times[\Theta(l(x)-z)\rho_l+\Theta(z-l(x))\rho_g]. \tag{3.14}$$

Inserting $\hat{\rho}(x,z)$ into Eq. (2.1) yields

$$\Omega([\hat{\rho}(x,z)];T,\mu;[\tilde{w}],[V])=\Lambda\Omega_b(\rho_g,T,\mu)+A\Omega_s(l_-;T,\mu;[\tilde{w}],[V])+L_y\Omega_l([l(x)];T,\mu;[\tilde{w}],[V]). \tag{3.15}$$

The surface contribution Ω_s (see Appendix B) is determined by the properties of the homogeneous, flat substrate w. Thus, in contrast to the SCS, here one only has to deal with one wetting transition on w at $T=T_w^-$. The wetting transition on the stripe part w_{st} is suppressed due to the finite lateral extension of the stripe.

The effect of the stripe on the liquid-vapor interface is captured by the line contribution to the free energy functional. This contribution reads

$$\Omega_l[l(x)]=\tau(d_w^\pm,l_-)+\tilde{\omega}[l(x)]. \tag{3.16}$$

Whereas $\tau(d_w^\pm,l_-)$ [see Eq. (B14)] is independent of $l(x)$, $\tilde{\omega}[l(x)]$ [see Eq. (B15)] is a functional of $l(x)$. Functional differentiation of $\Omega_l[l(x)]$, i.e., of $\tilde{\omega}[l(x)]$, yields the ELE

$$\Delta\Omega_b-\Delta\rho[\rho_l t(\overline{l}(x)-d_w^+)-V(x,\overline{l}(x))]-\Delta\rho\rho_l\int_{-a/2}^{a/2}dx'\int_{\overline{l}(x)-d_w^+}^{\overline{l}(x)-d_w^-}dz\;\overline{w}(x-x',z)+(\Delta\rho)^2\int_{-\infty}^{\infty}dx'\int_0^{\overline{l}(x')-\overline{l}(x)}dz'\;\overline{w}(x-x',z')=0. \tag{3.17}$$

The corresponding ELE within the local approximation $\tilde{\omega}_{\mathrm{loc}}[l(x)]$ of $\tilde{\omega}[l(x)]$ is

$$\Delta\Omega_b-\Delta\rho[\rho_l t(\overline{l}(x)-d_w^+)-V(x,\overline{l}(x))]-\Delta\rho\rho_l\int_{-a/2}^{a/2}dx'\int_{\overline{l}(x)-d_w^+}^{\overline{l}(x)-d_w^-}dz\,\overline{w}(x-x',z)-\frac{\sigma_{lg}\overline{l}''(x)}{[1+(\overline{l}'(x))^2]^{3/2}}=0. \tag{3.18}$$

In the following we always discuss the actual equilibrium liquid-vapor interface profiles; therefore, we omit the overbar.

IV. PROPERTIES OF THE INTERFACIAL PROFILES

A. Curvature behavior

Within the local theory the ELE's for the SCS, LCS, and CST determine the local curvature $K(x)$ of the planar curve $(x,l(x))$:

$$\sigma_{lg}K(x)=\frac{\sigma_{lg}l''(x)}{\{1+[l'(x)]^2\}^{3/2}}=U(x,l(x)), \tag{4.1}$$

with

$$U(x,z)=\Delta\Omega_b+\frac{\partial\omega(x,z;d_w^\pm)}{\partial z}+\mathcal{C}(x,z;d_w^\pm). \tag{4.2}$$

The ''local'' effective interface potential $\omega(x,z;d_w^\pm)$ is given by Eq. (B6). The function $\mathcal{C}(x,z;d_w^\pm)$ takes into account the difference between d_w^+ and d_w^-, i.e., it vanishes for $d_w^+=d_w^-$ and for $d_w^+\neq d_w^-$ in the limit $|x|\to\infty$ [see Eqs. (3.10) and (3.18)]. In the limit $|x|\to\infty$ the lines $z(x)$ defined implicitly by $U(x,z)=0$ asymptotically approach those values for which the function $\Delta\Omega_b l+\omega_\pm(l)$ [compare Eq. (B2)] is extremal with respect to l. One of these values corresponds to the global minimum and thus is the equilibrium film thickness $l_\pm$. In addition to this, there may be more extremal values depending on whether the system is at or off coexistence and on the type of wetting transition under consideration. Since $l(x)$ asymptotically approaches the values $l_\pm$ for $|x|\to\infty$, it also approaches the contour line given by $U(x,z)=0$ corresponding to the global minimum of $\Delta\Omega_b l+\omega_\pm(l)$. Figure 4 shows an example for the line $U(x,z)=0$ on a SCS and the corresponding interfacial profile $l(x)$ for a thermodynamic state along a complete wetting isotherm. The sign of the curvature is given by the sign of $U(x,z)$. The point where $l(x)$ and the line $U(x,z)=0$ inter-

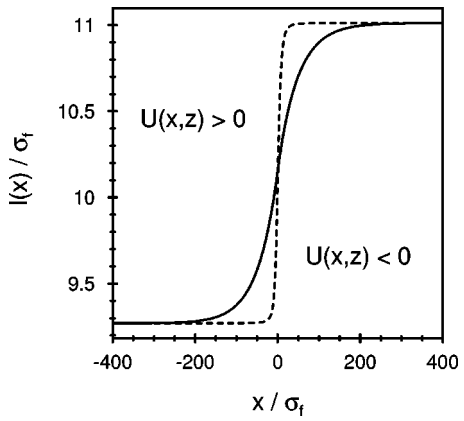

FIG. 4. Typical example for the shape of a liquid-vapor interface of a liquidlike film covering a SCS or LCS (full line) and the corresponding contour line $U(x,z)=0$ (dashed line) which separates regions with positive interface curvature ($K(x,z)=U(x,z)/\sigma_{lg}>0$) from regions with negative curvature ($K(x,z)<0$) [see Eqs. (4.1) and (4.2)]. The intersection between both lines is the turning point of the interface profile. The interface profile shown here is calculated for $T^*=k_BT/\epsilon_f=1.3$ and $\Delta\mu^*=\Delta\mu/\epsilon_f=10^{-3}$ and is also displayed in Fig. 7. The substrate is a SCS with the interaction parameters chosen such that the system exhibits critical wetting transitions at $T_w^{+}{}^*=1.0$ and $T_w^{-}{}^*=1.2$ on w_+ and w_-, respectively (compare Fig. 7). Therefore, along the complete wetting isotherm ($T^*=1.3,\Delta\mu$) the functions $\Delta\Omega_b l+\omega_\pm(l)$ corresponding to the homogeneous and flat substrates w_+ and w_- each exhibit only one extremal point, and there is only a single contour line $U(x,z)=0$ interpolating between these two extremal points.

sect is the turning point of the profile. Due to this curvature behavior the function $l(x)$ for a SCS or a LCS is monotonous. Analogously, for a CST, $l(x)$ is monotonous in each of the intervals $x<0$ and $x>0$.

In general the curvature behavior as predicted by the actual nonlocal theory is different from that obtained within the local approximation. However, in Ref. [62] we have demonstrated that the differences between the local and nonlocal results are negligible if the local curvature is small, as is the case for complete and critical wetting transitions. Therefore, although the behavior of the integral expression in Eqs. (3.8) and (3.17) is not analytically transparent, we expect the curvature behavior of the profiles upon approaching a critical or complete wetting transition to be practically the same within the nonlocal and the local theories.

B. Asymptotic behavior of the interface profiles

The asymptotic form of the substrate potential $V(|x|\to\infty,z)$ of a heterogeneous substrate gives rise to a behavior

$$l(|x|\to\infty)=l_\pm+\delta l(x) \quad \text{with} \quad \delta l(x)=\lambda\, x^{-\alpha} \tag{4.3}$$

of the interface profile with a characteristic exponent α. λ is the amplitude of the so-called van der Waals tails (VDWT) $\delta l(x)$, which can be determined analytically for all three substrate types SCS, LCS, and CST for those cases in which parts of the substrate, considered per se in the corresponding homogeneous limit, undergo a critical ($T\nearrow T_w^{\pm},\Delta\mu=0$) or a complete ($T>T_w^{\pm},\Delta\mu\searrow 0$) wetting transition. These results are based on the assumption that the system is sufficiently close to the wetting transition temperature or to two-phase coexistence such that $l(x)\gg d_w^{\pm}$, and thus

$$\Delta\Omega_b+\left.\frac{\partial\omega(x,l)}{\partial l}\right|_{l=l(x)}=I_{(\mathrm{loc})}(x,l(x)) \tag{4.4}$$

for all three substrate types. $\omega(x,l)$ is given by Eq. (B6) omitting the arguments $d_w^{\pm}$.

Since with $l(x)\gg d_w^{\pm}$, $l_\pm\gg d_w^{\pm}$, Eq. (4.4) can be used for inserting the ansatz $l(x)=l_\pm+\delta l(x)$ into its local version. Considering then the behavior of Eq. (4.4) for large $|x|$ and exploiting the fact that $l_\pm$, which corresponds to the limit $|x|\to\infty$, minimizes Eq. (B1), leads to the expansion

$$a\,\delta l(x)+bx^{-\alpha}=\sigma_{lg}\delta l''(x), \quad \alpha>0, \tag{4.5}$$

with coefficients a and b. The term $\sim x^{-\alpha}$ stems from the leading term in $V(|x|\to\infty)-V_\pm(z)$ [see Eqs. (3.2), (3.11), and (3.12)] which determines the value of α. The leading asymptotic behavior of the solution of Eq. (4.5) is given by

$$\delta l(x)=-\frac{b}{a}x^{-\alpha}. \tag{4.6}$$

Within the nonlocal theory the right-hand side is replaced by the leading order in the series expansion of the integral $I(x,l_\pm+\delta l(x))$:

$$a\,\delta l(x)+bx^{-\alpha}=I(x,l_\pm+\delta l(x))\sim x^{-\beta}, \quad \beta>0. \tag{4.7}$$

Thus the asymptotic solution $\delta l(x)$ in Eq. (4.7) for the VDWT is equal to that obtained within the local theory [Eq. (4.6)] if the right-hand side in Eq. (4.7) is subdominant as compared with the left-hand side, i.e., if $\beta>\alpha$. For $\beta=\alpha$ the amplitude λ [see Eq. (4.3)] obtained from the local theory differs from that following from the nonlocal one. It turns out that this is the case for the LCS. If one would have $\beta<\alpha$ which, however, is not the case here, even the exponent of the power-law decay of $\delta l(x)$ as obtained within the nonlocal theory would be different from that within the local theory, i.e., the VDWT would also differ qualitatively.

With the definition $l(x\to\pm\infty)=l_\pm\mp\delta l_\pm(x)$ for the SCS, it follows that

$$\delta l_\pm(x)=\lambda_{\mathrm{crit}}^{\pm}x^{-3} \quad \text{with} \quad \lambda_{\mathrm{crit}}^{\pm}=\pm\frac{l_\pm^4}{2}\frac{a_2^+-a_2^-}{a_2^\pm} \tag{4.8}$$

in the case of a critical wetting transition on the semi-infinite, homogeneous substrate w_+ or w_-. Along a complete wetting isotherm the result is the same up to a numerical factor:

$$\delta l_\pm(x)=\lambda_{\mathrm{comp}}^{\pm}x^{-3} \quad \text{with} \quad \lambda_{\mathrm{comp}}^{\pm}=\pm\frac{l_\pm^4}{6}\frac{a_2^+-a_2^-}{a_2^\pm}. \tag{4.9}$$

Both Eqs. (4.8) and (4.9) are valid within the local and the nonlocal theories, in agreement with Ref. [51]. For the LCS one finds a different power law which reflects the fact that for this type of substrate the lateral dependence of the potential enters only into the subdominant terms:

$$\delta l(x)=\lambda x^{-4}, \tag{4.10}$$

with

$$\lambda_{\rm crit}^{\pm}=\begin{cases}\dfrac{9}{32}\dfrac{l_{\pm}^4}{|a_2|}(a_3^+-a_3^-)\left(1-\dfrac{9}{2}t_3\dfrac{(\Delta\rho)^2}{|a_2|}\right) & \text{(nonlocal)}\\ \dfrac{9}{32}\dfrac{l_{\pm}^4}{|a_2|}(a_3^+-a_3^-) & \text{(local)}\end{cases} \tag{4.11}$$

and

$$\lambda_{\rm comp}^{\pm}=\begin{cases}\dfrac{3}{32}\dfrac{l_{\pm}^4}{a_2}(a_3^+-a_3^-)\left(1-3t_3\dfrac{(\Delta\rho)^2}{a_2}\right) & \text{(nonlocal)}\\ \dfrac{3}{32}\dfrac{l_{\pm}^4}{a_2}(a_3^+-a_3^-) & \text{(local).}\end{cases} \tag{4.12}$$

For both complete and critical wetting transitions, the local and the nonlocal theories yield the same power-law behavior but different amplitudes. Analogously, for the CST one finds $l(|x|\to\infty)=l_-+\delta l(x)$, where

$$\delta l(x)=\lambda_{\rm crit}x^{-4} \quad \text{with} \quad \lambda_{\rm crit}=-\frac{3a}{2g_x}l_-^4\frac{a_3^+-a_3^-}{a_2^-} \tag{4.13}$$

for critical wetting, and

$$\delta l(x)=\lambda_{\rm comp}x^{-4} \quad \text{with} \quad \lambda_{\rm comp}=\frac{a}{2g_x}l_-^4\frac{a_3^+-a_3^-}{a_2^-} \tag{4.14}$$

for a complete wetting transition on the substrate w. Thus the VDWT resolve the difference between the local and the nonlocal theories, for the LCS, but not for the SCS and CST.

On a laterally homogeneous and flat substrate the film thickness is given by $l_{\pm}=3a_3^{\pm}/2|a_2^{\pm}|$ for critical wetting, and by $l_{\pm}\sim(a_2^{\pm}/\Delta\mu)^{1/3}$ for complete wetting. For the derivation of the expressions for the VDWT, we have used Ruse relations which do not hold for $a_3^{\pm}=0$ in the case of critical wetting and $a_2^{\pm}=0$ in the case of complete wetting, respectively. In these cases of complete wetting at T_w or of tricritical wetting higher-order terms have to be taken into account in order to determine the amplitudes of the VDWT. Finally we note that due to the behavior of the curvature of $l(x)$ — as stated in Sec. IV A — the signs of the amplitudes of the VDWT are fixed by $\mathrm{sgn}(l_+-l_-)$.

C. Partial versus complete wetting of a chemical step

The SCS and LCS allow one to realize thermodynamic states for which one half of the substrate, say w_+, is completely wet, whereas the other half is only partially wet. Such a state is realized for $T_w^+<T_0<T_w^-$ and $\Delta\mu=0$. The corresponding interface profile does not depend on whether this state is reached along coexistence $(T\nearrow T_0,\Delta\mu=0)$ or along a complete wetting isotherm $(T=T_0,\Delta\mu\searrow 0)$ (see Fig. 5). The liquid-vapor interface attains a finite value l_- for $x\to-\infty$ and diverges for $x\to\infty$.

The characteristic length scale for lateral variations of the interfacial profile $l(x)$ is the lateral height-height correlation

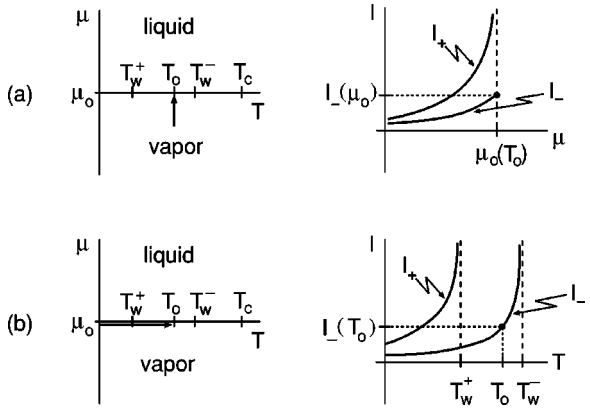

FIG. 5. Incomplete wetting of the substrate half $x<0$ and complete wetting of the substrate half $x>0$ can be obtained by approaching a thermodynamic state $(T_w^+<T_0<T_w^-,\Delta\mu=0)$ on different thermodynamic paths in the (T,μ) plane. This is illustrated by the corresponding schematic behavior of the equilibrium film thickness $l_{\pm}$. For reasons of simplicity, the coexistence curve $\mu_0(T)$ is straightened out. (a) Upon approaching $\mu_0(T_0)$ along the isotherm with $T_w^+<T_0<T_w^-$, l_+ diverges, whereas l_- remains finite. (b) If the temperature is increased along coexistence $\mu=\mu_0$, as T approaches T_w^+, l_+ diverges, and is macroscopically large for $T_w^+\leqslant T\leqslant T_0$. l_- also increases but remains finite since $T\leqslant T_0<T_w^-$. Both thermodynamic paths lead to the same final state $(T_0,\mu_0(T_0))$ of the system, and thus to the same interfacial profile $l(x;T_0,\mu_0(T_0))$. This is also true if the wetting transition at T_w^+ is first order; in this case in (b), l_+ would jump to infinity at $T=T_w^+$.

length $\xi_{\parallel}$. For complete wetting of the substrate $w_{\pm}$ this length is given by (compare Ref. [63])

$$\xi_{\parallel,\rm comp}^{\pm}=\sqrt{\sigma_{lg}}\left(\left.\frac{d^2\omega_{\pm}}{dl^2}\right|_{l=l_{\pm}}\right)^{-1/2}\underset{l_{\pm}\to\infty}{\to}\sqrt{\frac{\sigma_{lg}}{6a_2^{\pm}}}l_{\pm}^2$$
$$\sim(\Delta\mu)^{-2/3}, \tag{4.15}$$

whereas, for a critical wetting transition,

$$\xi_{\parallel,\rm crit}^{\pm}=\sqrt{\frac{\sigma_{lg}}{3a_3^{\pm}}}l_{\pm}^{5/2}\sim t_w^{-5/2}, \tag{4.16}$$

where $t_w=(T_w-T)/T_w$ (compare Ref. [64]). In the case that the substrate half w_+ undergoes complete wetting and the substrate half w_- incomplete wetting, we make the scaling ansatz

$$l(x,\Delta\mu)=l_+(\Delta\mu)f(x/\xi_{\parallel,\rm comp}^{+}(\Delta\mu)) \tag{4.17}$$

for the evolution of the profile $l(x,\Delta\mu>0)$ from a shape which attains the constant value l_+ in the limit $x\to\infty$ for $\Delta\mu>0$ to the shape for $\Delta\mu=0$ with $l(x\to\infty,\Delta\mu=0)=\infty$. With this ansatz and in the case when the slope of the profile is small such that the left-hand side of Eq. (3.10) can be replaced by its lowest-order expansion $\sigma_{lg}l''(x)$, one obtains the differential equation

$$1-f(y)^{-(\zeta-3)}=(\zeta-3)f''(y) \tag{4.18}$$

for the scaling function $f(y)$ when the attractive fluid-fluid and substrate-fluid interactions decay as $r^{-\zeta}$; $f(y\to\infty)=1$, independent of ζ. This demonstrates that the above scaling

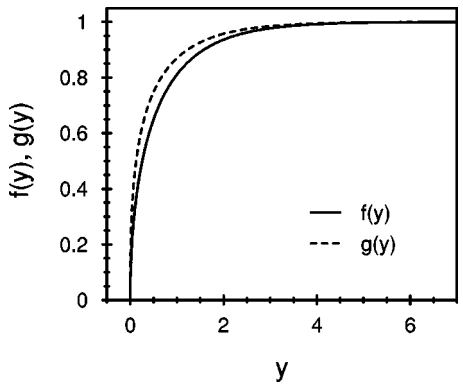

FIG. 6. Scaling functions f and g as defined by Eqs. (4.17) and (4.21) calculated for Lennard-Jones potentials ($\zeta=6$). The scaling function f governs the evolution of the interface profile if the thermodynamic state ($T_w^+<T_0<T_w^-, \Delta\mu=0$) at two-phase coexistence is approached along an isotherm ($T=T_0, \Delta\mu$); for this limiting thermodynamic state the substrate half $x>0$ of a SCS or LCS is completely wet, whereas the substrate half $x<0$ is only partially wet [see Fig. 5(a)]. Analogously, the evolution of the interfacial profile upon approaching a critical wetting transition at ($T_0=T_w^+<T_w^-, \Delta\mu=0$) along a path at coexistence, as shown in Fig. 5(b), is described by the scaling function g. In the limit $y\to 0$ one has $f(y\to 0)\sim y^{1/2}$ and $g(y\to 0)\sim y^{2/5}$. $f(y)$ and $g(y)$ attain the value 1 for $y\to\infty$ according to $f(y\to\infty)=1-6(\sqrt{3}-1)(\sqrt{3}+1)^{-1}e^{-3+\sqrt{3}}e^{-y}+O(e^{-2y})$ and $g(y\to\infty)=1-6e^{-3}e^{-y}+O(e^{-2y})$.

ansatz does indeed hold. In the limit $\Delta\mu\searrow 0$ which corresponds to $\xi_{\parallel,\mathrm{comp}}^+\to\infty$, i.e., $y\to 0$, from the asymptotic behavior of the solution of Eq. (4.18) it follows that

$$l(x\to\infty)=\gamma_{\mathrm{comp}}x^{2/(\kappa+1)}$$

$$\text{with}\quad \gamma_{\mathrm{comp}}=\left(\frac{(\kappa+1)^2a_\sigma^+}{2\sigma_{lg}}\right)^{1/(\kappa+1)}. \tag{4.19}$$

The coefficients in Eq. (4.19) are defined by the asymptotic behavior of the effective interface potential $\omega_+(l\to\infty)=a_\sigma^+l^{-\sigma}+a_\kappa^+l^{-\kappa}+\mathcal{O}(l^{-\kappa-1})$, where $\sigma=\zeta-4$ and $\kappa=\zeta-3$. For Lennard-Jones potentials, $\sigma=2$ and $\kappa=3$, so that

$$l(x\to\infty)=\left(\frac{8a_2^+}{\sigma_{lg}}\right)^{1/4}x^{1/2},\quad \Delta\mu=0, T_w^+<T<T_w^-. \tag{4.20}$$

This power law was predicted originally by de Gennes [55]; the expression for the amplitude is in accordance with Ref. [51]. Figure 6 shows the scaling function $f(y)$ for $\zeta=6$.

For the case $T\nearrow T_0=T_w^+$ with the critical wetting transition temperature T_w^+ on the substrate half w_+ and $\Delta\mu=0$, the scaling ansatz

$$l(x\to\infty,T)=l_+(T)g(x/\xi_{\parallel,\mathrm{crit}}^+(T)) \tag{4.21}$$

leads to the differential equation

$$g(y)^{-(\zeta-3)}-g(y)^{-(\zeta-2)}=g''(y) \tag{4.22}$$

for the scaling function $g(y)$, with $g(y\to\infty)=1$ independent of ζ. In the limit $T\nearrow T_w^+$, $\xi_{\parallel,\mathrm{crit}}^+(T)$ diverges, and from the behavior of the solution of Eq. (4.22) for $y\to 0$, one finds

$$l(x\to+\infty)=\gamma_{\mathrm{crit}}x^{2/(\kappa+2)}$$

$$\text{with}\quad \gamma_{\mathrm{crit}}=\left(\frac{(\kappa+2)^2a_\kappa^+}{2\sigma_{lg}}\right)^{1/(\kappa+2)} \tag{4.23}$$

for $T=T_w^+$, so that, for $\zeta=6$,

$$l(x\to\infty)=\left(\frac{25a_3^+}{2\sigma_{lg}}\right)^{1/5}x^{2/5},\quad \Delta\mu=0, T=T_w^+<T_w^-. \tag{4.24}$$

Figure 6 shows the scaling function $g(y)$ for $\zeta=6$.

All these equations hold both for the SCS with $a_2^+=(\Delta\rho/2)(u_3^+-t_3\rho_l)$ and $a_3^+=(\Delta\rho/3)(u_4^+-(t_4+3t_3d_w)\rho_l)$ and for the LCS with $a_2^+=(\Delta\rho/2)(u_3^H-t_3\rho_l)$ and $a_3^+=(\Delta\rho/3)(2(d+1)u_4^+-(2d+1)u_4^H-(t_4+3t_3d_w)\rho_l)$. The scaling functions f and g are independent of the thermodynamical parameters T and μ and of the amplitudes of the molecular interactions. These dependences are completely absorbed into $\xi_\parallel^+$ and l_+. However, f and g do depend on the exponent ζ of the power-law decay of the attractive interparticle potentials. We note that the scaling functions f and g do not take into account the lateral long-ranged VDWT of $l(x)$ (see Sec. IV B). These VDWT give rise to additional small corrections to the behavior of $f(y\to\infty)$ and $g(y\to\infty)$.

D. Partial versus complete wetting of a chemical stripe

A similar analytic calculation to that in Sec. IV C can be carried out for the case of a CST with the parameters chosen such that at coexistence $\Delta\mu=0$ and a fixed temperature $T_w^+<T<T_w^-$ the outer area is only partially wet whereas the stripe region is completely wet in the limit $a=\infty$. It turns out that the analytical solution for the shape of the profile in the case of large a is a semiellipse:

$$l(x;a\to\infty)=\sqrt{\frac{2}{a}}\left(\frac{2a_2^+}{\sigma_{lg}}\right)^{1/4}\sqrt{\frac{a^2}{4}-x^2}, \tag{4.25}$$

i.e., the half axes are $r_x=a/2$ and $r_z=(2a_2^+/\sigma_{lg})^{1/4}\sqrt{a/2}$. The corresponding excess coverage, in comparison with the case $a=0$, scales as $\Gamma_{\mathrm{ex}}(a\to\infty)\sim a^{3/2}$. In the limit $a\to\infty$ at both stripe boundaries $x=\pm a/2$, one recovers the square-root behavior given by Eq. (4.20). In this limit the presence of the second, distant boundary of the stripe gives rise to corrections to this square-root behavior of the interfacial profile:

$$l(x;a\to\infty)=\left(\frac{8a_2^+}{\sigma_{lg}}\right)^{1/4}\sqrt{x}\left[1-\frac{x}{2a}-\frac{x^2}{8a^2}+\mathcal{O}((x/a)^3)\right]. \tag{4.26}$$

The expression in Eq. (4.26) corresponds to a shifted coordinate system in which the two boundaries of the stripe are located at $x=0$ and $x=a\to\infty$.

E. Retardation

Due to retardation for large separations r dispersion interaction potentials decay as r^{-7} rather than r^{-6} [48]. These retardation effects become important for thick wetting layers. Therefore they have to be taken into account in the discussion of the VDWT and of the film morphology for the crossover between partially and completely wetted substrate parts. For homogeneous and planar substrates in the retarded regime the substrate potential decays as $V(z \gg \sigma_f) = -v_4 z^{-4} - v_5 z^{-5} + \mathcal{O}(z^{-6})$. If the interaction potential of the fluid particles is also retarded one has $t(z \gg \sigma_f) = -s_4 z^{-4} - s_5 z^{-5} + \mathcal{O}(z^{-6})$, so that the effective interface potential turns into

$$\omega(l \gg \sigma_f) = \frac{b_3}{l^3} + \frac{b_4}{l^4} + \mathcal{O}(l^{-5}) \tag{4.27}$$

with $b_3 = (\Delta\rho/3)(v_4 - s_4\rho_l)$ and $b_4 = (\Delta\rho/4)(v_5 - (s_5 + 4s_4 d_w)\rho_l)$. Thus for critical wetting $l(T \nearrow T_w) = -4b_4/3b_3$ with b_3 changing sign at $T = T_w$ and $l(\Delta\mu \searrow 0) = (3b_3/\Delta\Omega_b)^{1/4} \sim (\Delta\mu)^{-1/4}$ along a complete wetting isotherm.

The substrate potential of a SCS, $V(x,z) = V_{\rm att}(x,z) + V_{\rm rep}(x,z)$, with $V_{\rm att}(x,z)$ in accordance with Eq. (A8), approaches

$$V_{\rm att}(x \to \pm\infty, z) = -\frac{v_4^{\pm}}{z^4} + \frac{v_4^{+} - v_4^{-}}{2x^4} + \mathcal{O}(x^{-5}) \tag{4.28}$$

for large $|x|$. Equation (4.28) implies $\delta l_{\pm}(x) = l(x \to \pm\infty) - l_{\pm} \sim x^{-4}$ for the VDWT if the substrate $w_{\pm}$ undergoes a critical or complete wetting transition. Analogously, for the LCS and CST one finds $\delta l_{\pm}(x) = l(x \to \pm\infty) - l_{\pm} \sim x^{-5}$.

For $\zeta = 7$, Eqs. (4.19) and (4.23) imply

$$l(x \to \infty) = \left(\frac{25 b_3^{+}}{2\sigma_{lg}}\right)^{1/5} x^{2/5} \tag{4.29}$$

in the case of complete wetting of w_+ and partial wetting of w_- (i.e., $T_w^{+} < T_0 < T_w^{-}$ and $\Delta\mu = 0$) and

$$l(x \to \infty) = \left(\frac{18 b_4^{+}}{\sigma_{lg}}\right)^{1/6} x^{1/3} \tag{4.30}$$

at critical wetting (i.e., $T_w^{+} = T_0 < T_w^{-}$ and $\Delta\mu = 0$).

V. NUMERICAL ANALYSIS OF THE INTERFACE MORPHOLOGY

Although several properties of the liquid-vapor interfaces can be determined analytically, even within the sharp-kink approximation the behavior of $l(x)$ over the whole range of x values and for arbitrary values of T and μ can only be obtained numerically. Within the local theory for the SCS and LCS we solve the ELE given by Eq. (3.10); for the CST we solve the ELE given by Eq. (3.18). The corresponding analysis within the nonlocal theory requires that we numerically minimize the functional expression $\tilde{\omega}[l(x)]$ [see Eq. (B4)] instead of solving the corresponding ELE. The reason for this is that, as pointed out in Ref. [62], the numerical procedure for solving this nonlocal ELE leads to severe difficulties. In Ref. [62] the numerical techniques for calculating liquid-vapor interface profiles, and a comparison of the results as obtained within the nonlocal and the local theory, are described in detail. It turns out that in general these differences are very small. Therefore, in the following we focus on the numerical analysis of the local theory, keeping in mind that these results are practically indistinguishable from those following from the nonlocal theory although, in principle, the latter is the more reliable one.

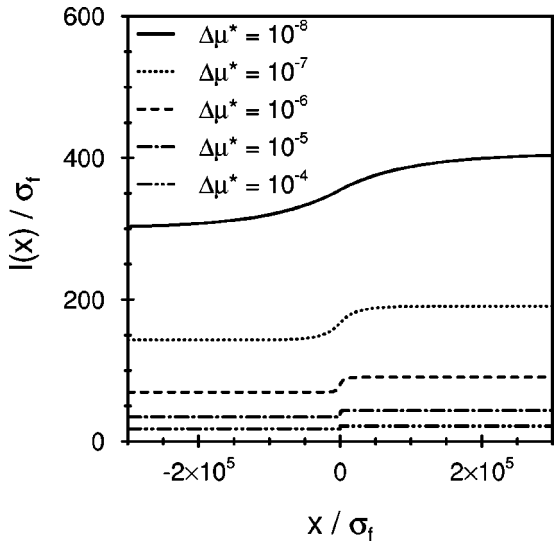

FIG. 7. Shape of the liquid-vapor interface profile on a SCS (see Fig. 2, with $n = \infty$) along an isotherm ($T^* = 1.3, \Delta\mu^*$), i.e., for complete wetting of both substrates w_+ and w_-. The parameters are chosen such that both substrates individually exhibit critical wetting transitions, w_+ at $T_w^* = 1.0$ and w_- at $T_w^* = 1.2$: $d_w^{\pm} = \sigma_f$, $u_3^{+} = 2.079\epsilon_f\sigma_f^3$, $u_4^{+} = 12.475\epsilon_f\sigma_f^4$, $u_{4,x}^{+} = u_4^{+} g_x/g_z = u_4^{+}$, and $u_9^{+} = 0.277\epsilon_f\sigma_f^9$, whereas $u_i^{-} = 0.809 u_i^{+}$. Therefore for the temperature chosen here at two-phase coexistence both substrate halves are completely wet. The profiles shown here remain practically unchanged if the local ELE in Eq. (3.10) is approximated further by the square-gradient expression in Eq. (5.1) or if the substrate potential $V(x,z)$ is replaced by the steplike substrate potential $V_\infty(x,z) = V_+(z)\Theta(x) + V_-(z)\Theta(-x)$.

A. Chemical step

Figure 7 displays profiles of liquid-vapor interfaces for a substrate with a chemical step undergoing complete wetting of both w_+ and w_-. The parameters of the interactions are chosen such that both substrates exhibit critical wetting transitions w_+ at $T_w^* = k_B T_w/\epsilon_f = 1.0$ and w_- at $T_w^* = 1.2$. The profiles of the liquid-vapor interfaces are calculated for $T^* = 1.3 > T_w^{\pm *}$ and different values of $\Delta\mu$. In the limit $\Delta\mu \to 0$ both asymptotic film thicknesses $l_{\pm}$ diverge according to $l_{\pm} \sim (\Delta\mu)^{-1/3}$. The interface profile is extremely broad; we note that the scales of the two axes differ by about three orders of magnitude.

The crossover of $l(x)$ from l_- to l_+ is governed by two characteristic length scales, one for each substrate half w_+ and w_-. Whereas along the isotherm the position $|x_0| \lesssim \sigma_f$ of the turning point remains practically unchanged, the two points x_+ and x_-, where the profile $l(x)$ deviates from its

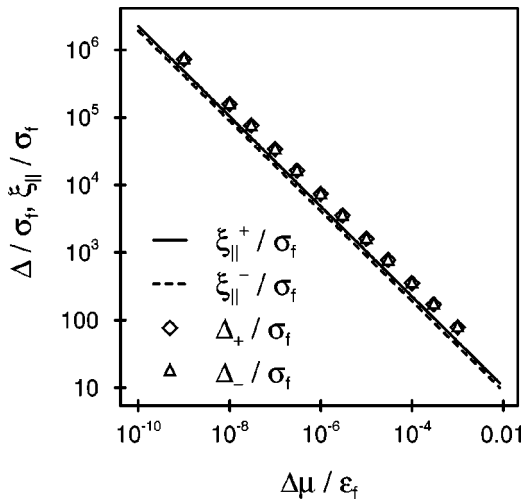

FIG. 8. Widths $\Delta_\pm$ of the interface profiles ($\diamond$,$\triangle$) shown in Fig. 7 compared with the lateral height-height correlation lengths $\xi_\parallel^\pm$ determined by $l_\pm$ [full and dashed line, Eq. (4.15)]. $\Delta_\pm$ is defined as that value $|x|$ at which $l(x)$ starts to deviate from its respective asymptote $l_\pm$ by 10% of $|l_+ - l_-|$, and measures the lateral extension of the transition region of the interface profile. For $\Delta\mu \to 0$ both $\Delta_\pm$ and $\xi_\parallel^\pm$ diverge according to $(\Delta\mu)^{-2/3}$, as expected for complete wetting transitions.

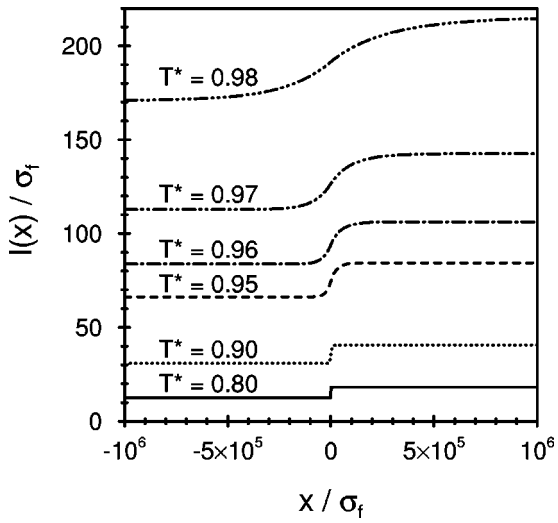

FIG. 9. Shape of the liquid-vapor interface profile of a liquidlike film across a SCS on a thermodynamic path at coexistence $\Delta\mu = 0$ with the temperature T^* increasing towards the wetting transition temperature $T_w^* = 1.0$ characteristic for *both* substrates $w_\pm$. The parameters are chosen such that the wetting transitions are continuous: $u_i^\pm$ and $u_{i,x}^\pm$ are equal to u_i^+ as in Fig. 7, but with $u_4^+ = u_{4,x}^+ = 14.035\epsilon_f\sigma_f^4$ and $d_w^\pm$ are also as in Fig. 7. Therefore $l_+(T) \neq l_-(T)$, although $T_w^+ = T_w^-$. Upon approaching the wetting transition temperature, both l_+ and l_- diverge as t_w^{-1} with $t_w = (T_w - T)/T_w$. As in Fig. 7 the results are practically insensitive against using the square-gradient approximation or using a steplike varying substrate potential. We note that here the scale of the x axis is about three times larger than in Fig. 7.

asymptotes by 10% of $|l_+ - l_-|$, diverge according to a power law. The characteristic length scale of the lateral variation of the profile is governed by the lateral interfacial height-height correlation length $\xi_\parallel$ given by Eq. (4.15). Figure 8 demonstrates that $x_\pm$ and $\xi_{\parallel,\mathrm{comp}}^\pm$ are proportional to each other.

Figure 9 shows liquid-vapor interface profiles calculated for a SCS which exhibits a critical wetting transition at $T_w^* = 1.0$ for both substrates w_- and w_+. The interface profiles have been obtained for different T along the thermodynamic path ($T \to T_w, \Delta\mu = 0$). As before, the position of the turning points remains fixed at $|x_0| \lesssim \sigma_f$, and the values of x_+ and x_- diverge for $T \to T_w$, i.e., $l_\pm \to \infty$. Here the divergence of $x_\pm$ is determined by $\xi_{\parallel,\mathrm{crit}}^\pm$ given by Eq. (4.16). From Fig. 10 it can be seen that also in the case of a critical wetting transition $x_\pm$ and $\xi_{\parallel,\mathrm{crit}}^\pm$ are proportional to each other.

The behavior of $l(|x| \to \infty)$ is ultimately determined by the VDWT given in Eqs. (4.8) and (4.9). However, it turns out that these power-law tails in $l(x)$ become relevant only for such large values of $|x|$ where in fact $\delta l(x)$ is smaller than the numerical error. Therefore the analytically known VDWT are numerically not accessible.

As demonstrated in Ref. [62] the more general nonlocal theory can be approximated by the corresponding local theory without losing significant quantitative accuracy. Since the slope dl/dx is small, one can go even a step further and within the local theory replace the expression $\sqrt{1+(dl/dx)^2} - 1$ by $(dl/dx)^2/2$, to be used in the local functional $\tilde{\omega}_{\mathrm{loc}}[l(x)]$ [see Eqs. (B4) and (B9)]. This gives rise to the ELE of a square-gradient theory:

$$\sigma_{lg} l''(x) = \Delta\Omega_b - \Delta\rho[\rho_l t(l(x) - d_w^+) - V(x, l(x))] + \Delta\rho\rho_l\{\overline{t}(x, l(x) - d_w^+) - \overline{t}(x, l(x) - d_w^-)\}, \tag{5.1}$$

which is the analog of a one-dimensional classical mechanical equation of motion in a time-dependent external potential. Moreover, as an additional approximation the actual substrate potential $V(x,z)$ with a smooth lateral variation of

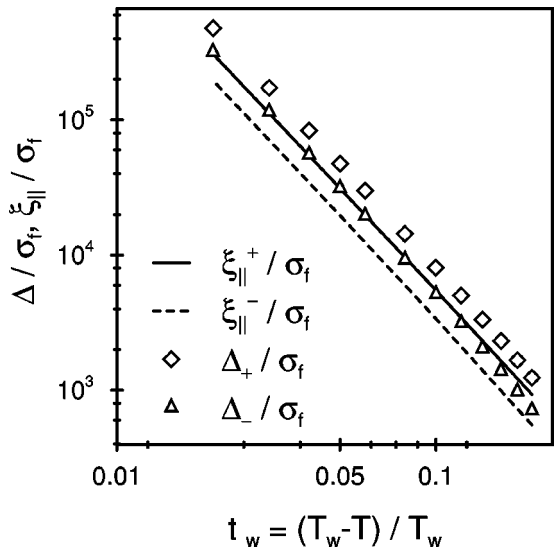

FIG. 10. Widths $\Delta_\pm$ of the interface profiles ($\diamond$,$\triangle$) corresponding to the profiles shown in Fig. 9 as compared with the lateral height-height correlation lengths $\xi_\parallel^\pm$ determined by $l_\pm$ [full and dashed lines, Eq. (4.16)]. $\Delta_\pm$ is defined as that value $|x|$ at which $l(x)$ starts to deviate from its respective asymptote $l_\pm$ by 10% of $|l_+ - l_-|$. Both $\Delta_\pm$ and $\xi_\parallel^\pm$ diverge as $t_w^{-5/2}$ for $t_w \to 0$, as expected for critical wetting transitions.

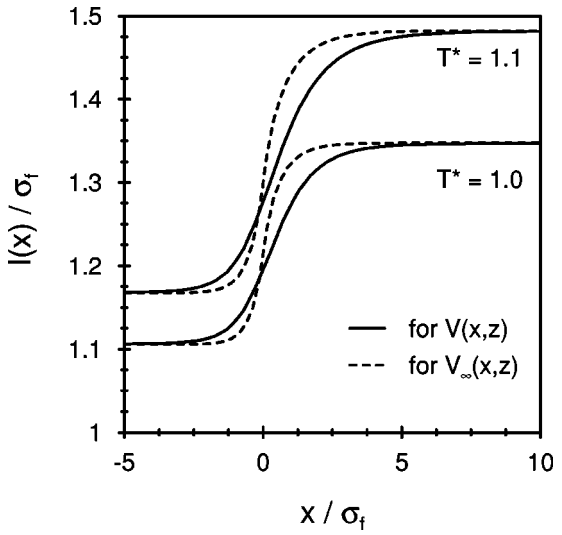

FIG. 11. Liquid-vapor interface profiles across a SCS with the parameters chosen such that both substrates individually exhibit first-order wetting transitions, the substrate w_- at $T_w^* \approx 1.314$ (with $d_w^- = \sigma_f$, $u_3^- = 2.513\epsilon_f\sigma_f^3$, $u_4^- = u_{4,x}^- = 3.770\epsilon_f\sigma_f^4$, and $u_9^- = 0.335\epsilon_f\sigma_f^9$) and the substrate w_+ at $T_w^* \approx 1.102$ (with $d_w^+ = 1.05\sigma_f$, $u_3^+ = 3.710\epsilon_f\sigma_f^3$, $u_4^+ = u_{4,x}^+ = 5.566\epsilon_f\sigma_f^4$, and $u_9^+ = 0.876\epsilon_f\sigma_f^9$). The system is at two-phase coexistence $\Delta\mu = 0$. The full and dashed lines correspond to the full smooth substrate potential $V(x,z)$ and its steplike approximation $V_\infty(x,z)$, respectively. In both cases the local ELE [Eq. (3.10)] and its square-gradient approximation [Eq. (5.1)] yield practically the same results.

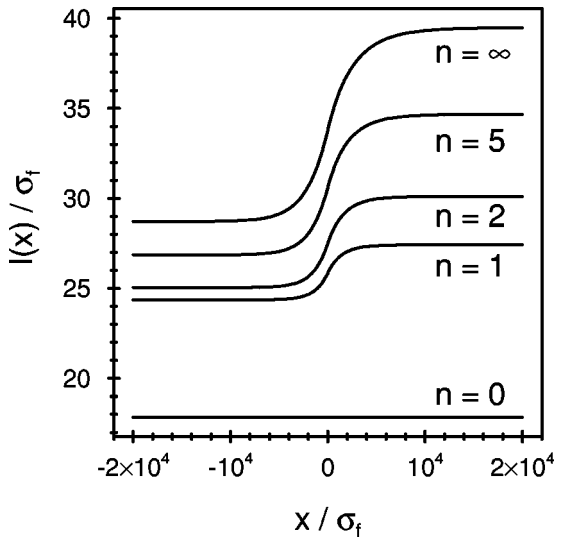

FIG. 12. Liquid-vapor interface profiles on a LCS for different numbers n of monolayers in the inhomogeneous surface layer. $n = 0$ corresponds to the homogeneous substrate w_H, whereas $n = \infty$ leads to a SCS with the substrate halves w_+ and w_-. d_w, u_i^H, and $u_{i,x}^H$ are chosen equal to d_w^-, u_i^-, and $u_{i,x}^-$ as in Fig. 7, respectively, such that both substrate halves exhibit a common critical wetting transition at $T_w^{+*} = T_w^{-*} = T_w^* = 1.2$. The interaction parameters of the surface layers are $u_i^+ = 1.1u_i^H$, $u_i^- = 1.05u_i^H$, and $g_x = g_z$. They do not affect the order of the wetting transition and its transition temperature, but they lead to a difference between $l_+(T)$ and $l_-(T)$. The temperature is fixed at $T^* = 1.1$, i.e., both substrate halves are only partially wet at coexistence $\Delta\mu = 0$. Moreover, we choose $\Delta\mu^* = 1.5\times10^{-6}$. As the number of monolayers in the surface layer n is increased, the interface profile for a SCS composed of w_+ and w_- evolves out of the flat profile for the homogeneous substrate w_H. Remarkably, a few adsorbed monolayers already have a pronounced effect on the wetting film.

$V_{\rm att}$ [Eqs. (A2) and (A3)] can be replaced by the steplike potential $V_\infty(x,z) = \Theta(-x)V_-(z) + \Theta(x)V_+(z)$. As it turns out, both approximations have only negligible effects on the numerical results for the interface profiles (see Figs. 7 and 9) because for thick wetting films the width of the profile $l(x)$ is much larger than the scale of the lateral variation of $V(x,z)$.

Figure 11 shows liquid-vapor interface profiles for a SCS whose parameters are chosen such that first-order wetting transitions occur at $T_w^* \approx 1.102$ and $T_w^* \approx 1.314$ on w_+ and w_-, respectively. Here the liquidlike layers are very thin. Therefore, the width of the profile is also rather small as compared to a system undergoing a critical or complete wetting transition. In this case the replacement of the smooth substrate potential $V(x,z)$ by the steplike potential $V_\infty(x,z)$ yields a detectable difference but without changing the qualitative behavior. Although the applicability of the present sharp-kink approximation for such thin films certainly deserves a caveat, we conclude that only in the case of a substrate potential, which gives rise to first-order wetting transitions, is the transition region of the interface profile on structured substrates confined to a region of the order of σ_f around the heterogeneity.

B. Chemical step within a surface layer

Section V A demonstrated that the properties of liquidlike wetting layers on a SCS heterogeneity are determined to a large extent by the asymptotic substrate potentials $V_\pm(z)$ of the semi-infinite substrate halves $x \lessgtr 0$. This is also the case for the LCS. The wetting properties of the substrate halves $x \lessgtr 0$ give rise to the asymptotic thickness of the wetting layer $l(x \to \pm\infty) = l_\pm$, as discussed in Sec. II C, and $l(x)$ smoothly and monotonously interpolates between them. Figure 12 displays a typical example of the influence of the thickness of the surface layer n on the profiles $l(x)$. This system exhibits a critical wetting transition at $T_w^{+*} = T_w^{-*} = T_w^* = 1.2$; we choose $T^* = 1.1$ and $\Delta\mu^* = 1.5\times10^{-6}$. Without an overlayer (i.e., the number of inhomogeneous surface layers $n = 0$) the system corresponds to the homogeneous and planar substrate w_H. As n is increased there is a crossover of $l(x)$ to the profile of a SCS. The typical profile widths are — as for the SCS — given by Eqs. (4.15) and (4.16) if one of the substrate halves exhibits a complete or a critical wetting transition, respectively. In the case of a first-order wetting transition, i.e., for thin liquidlike layers the deviation of $l(x)$ from its asymptotes is confined to a region of the order of σ_f around $x = 0$.

From the analytical results for the VDWT one expects that the profile $l(x)$ for a LCS approaches its asymptotes $l_\pm$ faster than in the case of a SCS, i.e., via $\delta l(|x| \to \infty) \sim x^{-4}$ [see Eqs. (4.10)—(4.12)] rather than x^{-3} [Eqs. (4.8) and (4.9)]. However, since as observed above, the VDWT become relevant only for very large values of $|x|$ without affecting the main deviation of $l(x)$ from $l_\pm$ around $x = 0$, this more rapid decay is analytically accessible but does not play an important role for the overall behavior of $l(x)$.

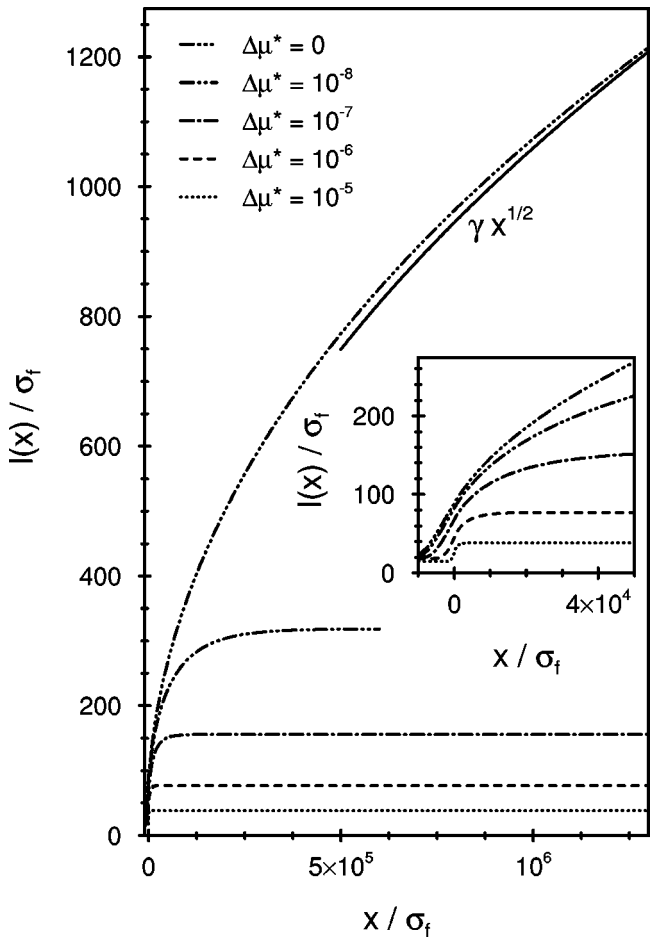

FIG. 13. Liquid-vapor interface profiles across a LCS with the substrate half $x>0$ completely wet and the substrate half $x<0$ only partially wet. The parameters d_w, u_i^H, u_i^+, and g_x/g_z are chosen as in Fig. 12, $u_i^- = 0.75u_i^H$, and we consider $n=10$ inhomogeneous monolayers. With this choice of parameters the substrate half $x>0$ exhibits a critical wetting transition at $T_w^{+}{}^* = 1.2$ whereas the substrate half $x<0$ undergoes a weakly first-order wetting transition at $T_w^{-}{}^* \approx 1.306$, with the thickness l_- of the liquidlike film of the order of $10\sigma_f$ in the vicinity of $T_w^{-}{}^*$. The temperature is fixed at $T^*=1.3$ such that at coexistence $\Delta\mu=0$ the substrate half $x<0$ remains partially wet. At coexistence, $l(x)$ diverges according to $l(x\to\infty)=\gamma_{\rm comp}x^{1/2}$ [see Eqs. (4.19) and (4.20)]. As in the case of the SCS, the width Δ_+ of the interface profile for $x>0$ diverges according to $(\Delta\mu)^{-2/3}$ for $\Delta\mu\to 0$; Δ_- remains finite even at $\Delta\mu=0$, for which it is of the order of $\xi_\parallel^- \sim 10^4\sigma_f$. The inset provides a magnified view of the region around $x=0$. For $\Delta\mu\to 0$ and $x\to\infty$ the profiles exhibit scaling and are governed by the same scaling function $f(y)$ as the SCS [Eq. (4.17)].

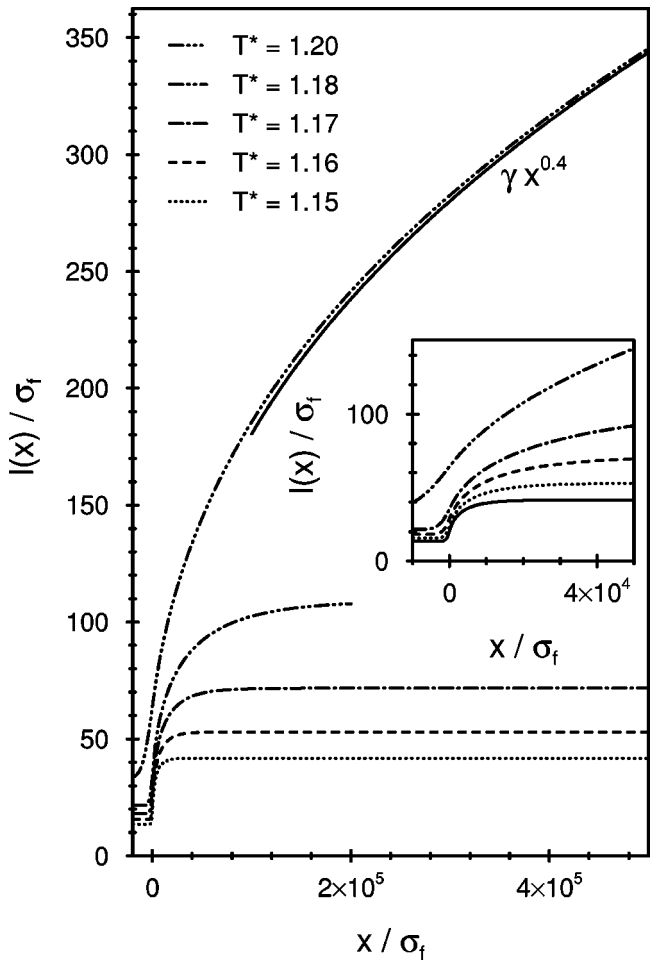

FIG. 14. Liquid-vapor interface profiles across a LCS along a thermodynamic path at coexistence $\Delta\mu=0$ approaching the critical wetting transition temperature $T_w^{+}{}^*=1.2$ of the substrate half $x>0$. Here we choose the same values of d_w, u_i^H, and g_x/g_z as in Figs. 12 and 13: $u_i^+ = u_i^H$ and $u_i^- = 0.92u_i^H$. The latter choice induces a weakly first-order wetting transition on the substrate half $x<0$ at $T_w^* \approx 1.216$ with a thickness of the liquidlike wetting film of the order of $10\sigma_f$ slightly below the transition temperature. In the limit $T\nearrow T_w^+$, $l_+(T)$ diverges as $(T_w^+ - T)^{-1}$, whereas $l_-(T)$ remains finite. At $T=T_w^+$ one has the power-law behavior $l(x\to\infty) = \gamma_{\rm crit}x^{2/5}$ [see Eqs. (4.23) and (4.24)]. As in the case of the SCS, the width Δ_+ of the interface for $x>0$ diverges as $t_w^{-5/2}$, with $t_w = (T_w^+ - T)/T_w^+ \to 0$, whereas Δ_- remains finite even at $t_w=0$, where it is of the order of $\xi_\parallel^- \sim 10^4\sigma_f$. The inset provides a magnified view of the region around $x=0$. For $t_w\to 0$ and $x\to\infty$ the profiles exhibit scaling and are governed by the same scaling function $g(y)$ as the SCS [Eq. (4.21)].

The divergence of the function $l(x)$ for $x\to\infty$, when the substrate half $x>0$ is completely wet and the other substrate half $x<0$ is only partially wet, is given by Eqs. (4.19) and (4.23) for $T>T_w^+$ and $T=T_w^+$, respectively. This behavior is shown in Figs. 13 and 14. The asymptotic behavior for $x>0$ of the profiles for small $\Delta\mu$ and small $T_w - T$, respectively, is in excellent agreement with the numerical solutions of Eqs. (4.18) and (4.22).

C. Chemical stripe

First we analyze a CST for which the homogeneous substrate w corresponding to the embedding substrate undergoes a critical wetting transition at $T_w^*=1.2$, whereas the homogeneous substrate corresponding to the inserted slab $w_{\rm st}$ exhibits a critical wetting transition at $T_w^*=1.0$. We consider thermodynamic states along the complete wetting isotherm ($T^*=1.1,\Delta\mu$), so that at coexistence the substrate as a whole is only partially wet. The complete wetting transition on $w_{\rm st}$ is suppressed by the finite lateral extension of $w_{\rm st}$.

Figure 15 displays liquid-vapor interface profiles for different values of $\Delta\mu$. The width of the transition regions at $x=\pm a/2$ increases as $\Delta\mu$ becomes smaller. If this width is small compared with the width a of the stripe region, the profile $l(x)$ attains the equilibrium film thickness l_+ on the

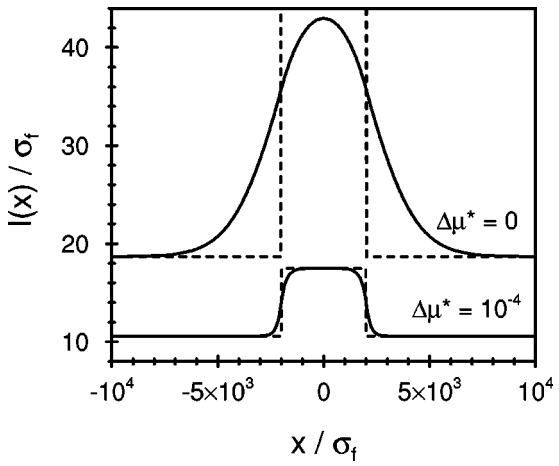

FIG. 15. Liquid-vapor interface profiles on a CST (full lines). The slab w_{st} is symmetric around $x=0$, and forms a chemical stripe at the substrate surface with a width $a/\sigma_f=4000$. The parameters for the substrate potential are chosen as in Fig. 7, i.e., the whole substrate undergoes a critical wetting transition at $T_w^*=1.2$. The critical wetting transition at $T_w^*=1.0$ corresponding to the slab w_{st} is suppressed due to the finite lateral extension of the slab. The profiles correspond to the temperature $T^*=1.1$ so that at coexistence $\Delta\mu=0$ the inhomogeneous substrate as a whole is only partially wet. Upon approaching coexistence $\mu\to\mu_0$ the interface profile broadens. The dashed lines indicate the equilibrium film thicknesses corresponding to the flat and homogeneous + and − substrate; $l_+=\infty$ for $\Delta\mu=0$. If the width Δ_+ of the transition regions near $|x|=a/2$ is small compared to a (as it is the case for $\Delta\mu^*=10^{-4}$), one has $l(x)\approx l_+$ in the middle of the stripe.

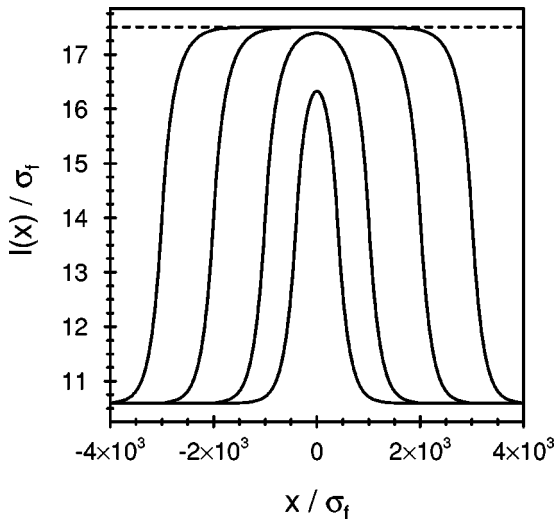

FIG. 16. Change of the morphology of the liquid-vapor interface profiles on a CST upon a variation of the stripe width a. The profiles correspond to $a/\sigma_f=800$, 2000, 4000, and 6000 from the inner profile to the outer profile. The temperature T and the interaction potentials are chosen as in Fig. 15 and $\Delta\mu^*=10^{-4}$, i.e., the interface profile for $a=4000\sigma_f$ is the same as in Fig. 15. If the stripe width is decreased the region where $l(x)$ attains the equilibrium film thickness l_+ (indicated by the dashed line) shrinks and ultimately disappears. Only for $a\gg a_0$, where $a_0\approx 2\Delta_+(l_+)$ is a characteristic crossover width, does $l(x=0)$ attains the value l_+. One has $\Delta_+\sim\xi_\parallel^+$ (compare Fig. 8) and $\xi_\parallel^+=\sqrt{\sigma_{lg}/6a_2^+}l_+^2$ in the limit $\Delta\mu\to 0$, i.e., $l_+\to\infty$ [see Eq. (4.15)]. For the present system, $\xi_\parallel^+\approx 470\sigma_f$ and $a_0\approx 750\sigma_f$.

stripe area. Therefore, if a is large the profile for a CST is approximately composed of two interfacial profiles corresponding to two SCS's located at $x=-a/2$ and $x=+a/2$. As the stripe width a is decreased for fixed values of T and $\Delta\mu$ the region where $l(x)$ attains the value l_+ decreases, and ultimately vanishes as a becomes smaller than the width of the transition region. This behavior is shown in Fig. 16.

Figure 17 presents interface profiles for a CST with the chemical species of the slab and the surrounding substrate exchanged. Therefore, the substrate exhibits a critical wetting transition at $T_w^*=1.0$, and it is already completely wet at coexistence as the temperature is raised toward $T^*=1.2$. The latter is the transition temperature of the critical wetting transition on the homogeneous substrate corresponding to w_{st}. If we choose $T^*=1.1$ and decrease $\Delta\mu$, the whole substrate undergoes a complete wetting transition and the ''dent'' induced by the existence of the stripe-shaped heterogeneity is smeared out.

The above analysis demonstrates that the liquid leaks out of the chemical stripe if, on the embedding material, the fluid is close to a complete or critical wetting transition. Figure 18 shows that this leaking is absent if, on the embedding material, the fluid can form only a thin wetting film. This situation prevails if the outer material leads to a first-order wetting transition at T_w^-, and the temperature is chosen such that $T<T_w^-$. Figure 18 corresponds to a CST for which the slab as a homogeneous substrate also undergoes a first-order wetting transition at T_w^+, with $T_w^+<T<T_w^-$. The confinement of the liquid to the stripe is achieved both off and at two-phase coexistence. In view of practical applications of chemically structured surfaces in the context of microfluidics, this reveals for which materials and for which thermodynamic states a good performance without leakage can be expected.

In the strict sense of thermal equilibrium, so far only a few solid-fluid systems are known to exhibit a true first-order wetting phase transition at coexistence (e.g., He^4 on Cs [65,66]); up to now critical wetting has been observed only on fluid substrates (e.g., alkanes on aqueous solutions of salt or glucose [67,68]). The generic case is that fluids wet substrates completely above the triple point [50,69]. Although our theoretical framework is based on equilibrium statistical mechanics, the present model calculations for the morphology of wetting films can also be applied directly to nonvolatile liquids as long as their interaction with solid substrates can be modeled by an appropriate effective interface potential $\omega_\pm(l)$. Alternatively, these potentials can be inferred empirically from suitable experiments (see, e.g., Refs. [70,71]). In this sense our conclusions are valid also for nonvolatile liquids adsorbed on ''hydrophilic'' or ''hydrophobic'' parts of an inhomogeneous substrate, for which a wide range of wettability characteristics, beyond the strict equilibrium conditions, can be arranged.

The line tension $\tau_{CST}(a)$ associated with a chemical stripe can be written

$$\tau_{CST}(a)=a(\sigma_{w_+g}-\sigma_{w_-g})+2\tau_{SCS}+\delta\tau(a), \qquad (5.2)$$

where $\sigma_{w_\pm g}$ is the surface tension of the homogeneous + or − substrate in contact with the vapor, τ_{SCS} is the line tension associated with a single SCS, and $\delta\tau(a)$ with, as it turns out,

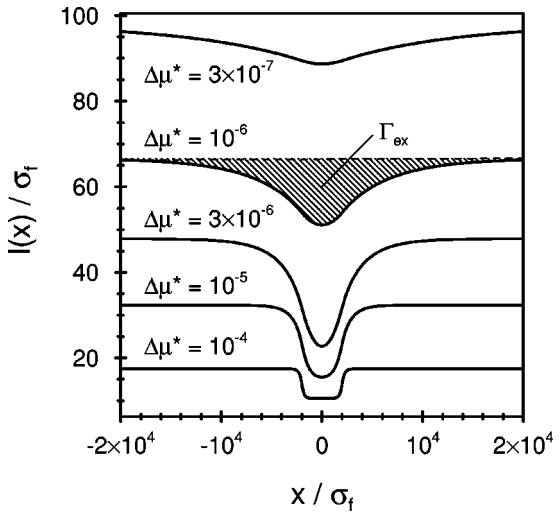

FIG. 17. Morphology of liquid-vapor interface profiles on a SST with the same parameters as in Fig. 15 but with the chemical species of the stripe and the surrounding region exchanged such that the slab w_{st} favors *thinner* liquidlike films than the embedding substrate. Since the temperature $T^*=1.1$ is above the wetting transition temperature corresponding to the outer region the substrate as a whole is completely wet at coexistence $\Delta\mu=0$. Upon approaching coexistence the equilibrium film thickness l_- corresponding to the surrounding substrate diverges, and the ''dent'' induced by the presence of the stripe deepens, though finally it is smeared out and vanishes. Upon decreasing $\Delta\mu$, the depth $l_- - l(x=0)$ of the ''dent'' first increases, then reaches a maximum value $[l_- - l(0)]_{\max} \approx 25\sigma_f$ at $\Delta\mu^* \approx 3\times 10^{-6}$, and finally vanishes as $(\Delta\mu)^{2/5}$ for $\Delta\mu \searrow 0$. Since the width of the dent is governed by the lateral correlation length $\xi_{\parallel,\mathrm{comp}}^-(\Delta\mu)$ which diverges as $(\Delta\mu)^{-2/3}$, the depletion of the coverage $|\Gamma_{\mathrm{ex}}| \sim (l_- - l(0))\xi_{\parallel,\mathrm{comp}}^-$ induced by the stripe *diverges* as $(\Delta\mu)^{-4/15}$.

$\delta\tau(a\to\infty)\sim a^{-2}$ is the effective interaction between the two line structures a distance a apart from each other. $\tau_{\mathrm{CST}}(a)$ generates a lateral force per unit length,

$$f(a) \equiv -\frac{\partial \tau_{\mathrm{CST}}(a)}{\partial a}, \tag{5.3}$$

acting on the stripe, and leading to a compression or dilation which is balanced by the elastic forces of the substrate. $f(a)$ is defined such that a positive sign corresponds to a dilation of the stripe. Our numerical results show that for large stripe widths and independent of the wetting characteristics of the materials under consideration $f(a)$ is practically constant with $f(a)=\sigma_{w_-g}-\sigma_{w_+g}+O(a^{-3})$; i.e., in Eq. (5.2) for $a \gtrsim 4\sigma_f$, the first contribution is the dominating one (see Fig. 19). For solid substrates the force is expected to have practically no effect because the compressibility of the substrate is very small. However, for fluid substrates such as fluids covered with Langmuir-Blodgett films, the force can have a significant effect. Therefore we propose to test this effective force between line structures by adsorbing liquidlike wetting films on a liquid substrate decorated with a Langmuir-Blodgett film which contains a stripe of different material. The adsorbed wetting films will cause a change in the stripe width depending on the compressibility of the Langmuir-Blodgett films. Moreover, such experimental arrangements

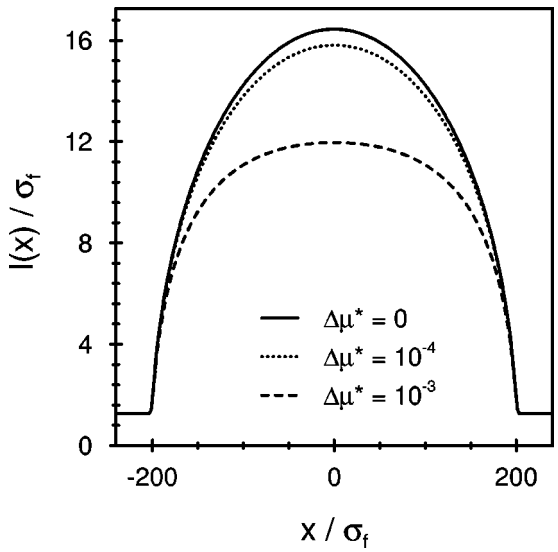

FIG. 18. Liquid-vapor interface profiles on a CST which undergoes a first-order wetting transition for a choice of temperature such that the substrate corresponding to w_{st} is completely wet (''hydrophilic''), whereas the embedding substrate is only partially wet (''less hydrophilic''). The parameters are chosen as in Fig. 11. Therefore the outer region undergoes a first-order wetting transition at $T_w^{-*} \approx 1.314$, whereas the homogeneous substrate corresponding to w_{st} exhibits a first-order wetting transition at $T_w^{+*} \approx 1.102$. The temperature is taken as $T^*=1.2$, so that $T_w^+ < T < T_w^-$. The width of the stripe is $a=400\sigma_f$, and the chemical potential is varied. Since the equilibrium film thickness $l_- = l(|x|\to\infty)$ is of the order of σ_f, the liquidlike ''channel'' is confined to the ''hydrophilic'' stripe region without leaking. The shape of the liquidlike channel for $\Delta\mu=0$ is in good agreement with the semiellipticc shape given by Eq. (4.25). If the stripe width a is increased, $l(x=0)$ and $l(x=0) - l_-$ increase as $a^{1/2}$, and the excess coverage supported by the stripe diverges as $\Gamma_{\mathrm{ex}} \sim a^{3/2}$.

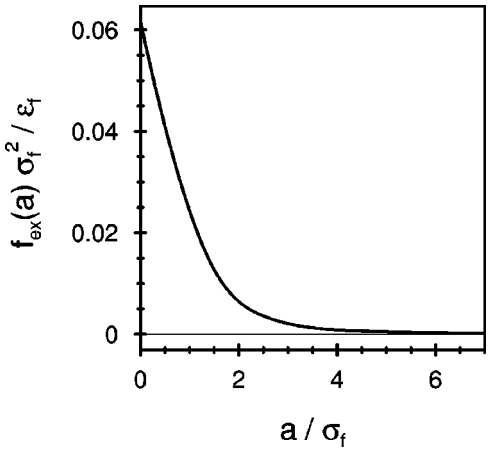

FIG. 19. Excess contribution $f_{\mathrm{ex}}(a) = -\partial\delta\tau(a)/\partial a$ to the force per unit length which acts on a chemical stripe. The system is the same as in Fig. 18 but with $T^*=1.0$, and at two-phase coexistence $\Delta\mu=0$. The total force is $f(a)=f_0+f_{\mathrm{ex}}(a)$, i.e., it is the sum of $f_{\mathrm{ex}}(a)$ and the constant contribution $f_0=\sigma_{w_-g}-\sigma_{w_+g}$ which in the present example is $f_0 \approx 0.137\epsilon_f/\sigma_f^2$. In the limit $a\to\infty$ $f_{\mathrm{ex}}(a)$ decays as a^{-3}. Both f_0 and f_{ex} are positive, leading to a dilation of the stripe.

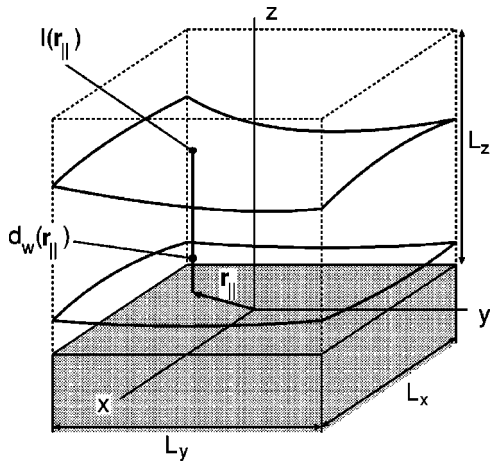

FIG. 20. Sketch of a fluid film on a general chemical inhomogeneity. The potential $V(\mathbf{r}_\parallel,z)$ of the arbitrarily structured substrate [with $\mathbf{r}_\parallel=(x,y)$] gives rise to a laterally varying exclusion length $d_w(\mathbf{r}_\parallel)$ and a liquid-vapor interface shape described by $l(\mathbf{r}_\parallel)$. The surface $[\mathbf{r}_\parallel,z=l(\mathbf{r}_\parallel)]$ separates the liquidlike wetting layer (below) from the bulk vapor phase (above). The system is truncated at $x=\pm L_x/2$, $y=\pm L_y/2$, and $z=L_z$ in order to facilitate the proper thermodynamic limit. (This truncation gives rise to artificial surface and line tensions generated by these boundaries.) The chemical inhomogeneity of the substrate is not indicated.

would facilitate probing our predictions concerning critical wetting transitions, as reported in Refs. [67] and [68], on chemically structured substrates.

VI. GENERAL MODEL FOR CHEMICALLY HETEROGENEOUS SUBSTRATES

It is possible to generalize the methods developed within the previous sections to substrates with arbitrary heterogeneities. The only required input is the substrate potential, which in general is a function $V(\mathbf{r})$ of all coordinates $\mathbf{r}=(\mathbf{r}_\parallel,z)=(x,y,z)$, and approximately follows from the summation of pair potentials. The substrate potential $V(\mathbf{r})$, together with the fluid-fluid interaction, gives rise to an interface profile $l(\mathbf{r}_\parallel)$, which in general depends on both lateral coordinates $\mathbf{r}_\parallel=(x,y)$ (see Fig. 20). We assume that the substrate is flat and located in the half space $w=\{\mathbf{r}\in\mathbb{R}^3|z\leqslant 0\}$. We take into account the excluded volume at the substrate surface by introducing a spatially varying $d_w(\mathbf{r}_\parallel)$. The insertion of the sharp-kink density profile

$$\hat{\rho}(\mathbf{r})=\Theta(z-d_w(\mathbf{r}_\parallel))[\Theta(l(\mathbf{r}_\parallel)-z)\rho_l+\Theta(z-l(\mathbf{r}_\parallel))\rho_g] \tag{6.1}$$

into Eq. (2.1), and the decomposition of $\Omega[\hat{\rho}]$ into bulk and subdominant contributions, yields

$$\Omega[\hat{\rho}(\mathbf{r})]=\Lambda\Omega_b(\rho_g;T,\mu)+\Omega_s([l(\mathbf{r}_\parallel)];T,\mu;[\tilde{w}],[V]). \tag{6.2}$$

Concerning the expression for Ω_s, we consider the thermodynamic limit and omit artificial contributions which stem from the truncation of the system. $\Lambda=L_xL_yL_z$ is the volume filled with fluid particles, and Ω_b is the free energy density of the bulk vapor phase [see Eq. (2.7)]. The subdominant contribution in Eq. (6.2) reads

$$\begin{aligned}\Omega_s[l(\mathbf{r}_\parallel)]=\int_A d^2r_\parallel\{&\Delta\Omega_b l(\mathbf{r}_\parallel)+\sigma_{wl}(\mathbf{r}_\parallel;d_w(\mathbf{r}_\parallel))\\&+\Sigma_{lg}(\mathbf{r}_\parallel,[l(\mathbf{r}_\parallel)])+\omega(\mathbf{r}_\parallel,l(\mathbf{r}_\parallel);d_w(\mathbf{r}_\parallel))\\&+\mathcal{C}(\mathbf{r}_\parallel,l(\mathbf{r}_\parallel);[d_w(\mathbf{r}_\parallel)])\},\end{aligned} \tag{6.3}$$

where

$$\begin{aligned}\sigma_{wl}(\mathbf{r}_\parallel;d_w(\mathbf{r}_\parallel))=&-\frac{\rho_l^2}{2}\int_0^\infty dz\ t(z)+\rho_l\int_{d_w(\mathbf{r}_\parallel)}^\infty dz\ V(\mathbf{r})\\&-d_w(\mathbf{r}_\parallel)\Omega_b^{(l)}\end{aligned} \tag{6.4}$$

can be interpreted as a local, spatially varying wall-liquid surface tension. Equation (6.4) is a generalization of Eq. (2.17). $\Sigma_{lg}(\mathbf{r}_\parallel,[l(\mathbf{r}_\parallel)])$ is the surface free energy density containing the cost in free energy for deforming the liquid-vapor interface:

$$\begin{aligned}\Sigma_{lg}^{(\mathrm{nloc})}(\mathbf{r}_\parallel,[l(\mathbf{r}_\parallel)])=&\sigma_{lg}-\frac{(\Delta\rho)^2}{2}\\&\times\int_A d^2r'_\parallel\int_0^\infty dz\int_0^{l(\mathbf{r}_\parallel)-l(\mathbf{r}'_\parallel)}\\&\times dz'\tilde{w}(|\mathbf{r}_\parallel-\mathbf{r}'_\parallel|,|z-z'|)\end{aligned} \tag{6.5}$$

within the nonlocal theory, and

$$\Sigma_{lg}^{(\mathrm{loc})}(\mathbf{r}_\parallel,[l(\mathbf{r}_\parallel)])=\sigma_{lg}\sqrt{1+(\nabla_\parallel l(\mathbf{r}_\parallel))^2} \tag{6.6}$$

within the local theory, with $\nabla_\parallel\equiv(\partial_x,\partial_y)$. The latter expression is the leading term of the gradient expansion of $\Sigma_{lg}^{(\mathrm{nloc})}$. In Eqs. (6.5) and (6.6) Σ_{lg} does not depend on the absolute value of $l(\mathbf{r}_\parallel)$ measured from the substrate surface, but only on the relative differences $l(\mathbf{r}_\parallel)-l(\mathbf{r}'_\parallel)$ so that σ_{lg} is independent of $l(\mathbf{r}_\parallel)$. Such additional dependences are brought about by replacing the sharp-kink density profile in Eq. (6.1) by a smooth one whose tails are cut off by the surface (see, e.g., Refs. [72] and [73]). As a generalization of Eq. (B6),

$$\begin{aligned}\omega(\mathbf{r}_\parallel,l(\mathbf{r}_\parallel);d_w(\mathbf{r}_\parallel))=&\Delta\rho\rho_l\int_{l(\mathbf{r}_\parallel)-d_w(\mathbf{r}_\parallel)}^\infty dz\ t(z)\\&-\Delta\rho\int_{l(\mathbf{r}_\parallel)}^\infty dz\ V(\mathbf{r})\end{aligned} \tag{6.7}$$

is the ''local'' effective interface potential for the effective interaction between the substrate surface and the liquid-vapor interface. Finally,

$$\mathcal{C}(\mathbf{r}_\parallel, l(\mathbf{r}_\parallel);[d_w(\mathbf{r}_\parallel)]) = -\frac{\rho_l^2}{2}\int_0^\infty dz\ t(z) + \rho_l \Delta\rho \int_{d_w(\mathbf{r}_\parallel)-l(\mathbf{r}_\parallel)}^\infty dz t(z) + \frac{\rho_l^2}{2}\int_A d^2 r'_\parallel \int_{d_w(\mathbf{r}_\parallel)-d_w(\mathbf{r}'_\parallel)}^\infty dz \int_z^\infty dv\ \tilde{w}(|\mathbf{r}_\parallel - \mathbf{r}'_\parallel|, |v|)$$
$$- \rho_l \Delta\rho \int_A d^2 r'_\parallel \int_{d_w(\mathbf{r}'_\parallel)-l(\mathbf{r}_\parallel)}^\infty dz \int_z^\infty dv\ \tilde{w}(|\mathbf{r}_\parallel - \mathbf{r}'_\parallel|, |v|) \tag{6.8}$$

takes into account the effects due to the lateral variation of $d_w(\mathbf{r}_\parallel)$. $\mathcal{C}$ vanishes for $d_w(\mathbf{r}_\parallel) \equiv d_w = \text{const}$.

If the substrate contains inhomogeneities with large linear extensions, i.e., the substrate is translationally invariant along one of the lateral directions, the subdominant contribution Ω_s decomposes into ''true'' surface and line contributions as discussed above for the SCS, LCS, and CST. In the absence of such an additional translational symmetry one cannot identify a genuine line contribution.

The equilibrium liquid-vapor interface profile $\overline{l}(\mathbf{r}_\parallel)$ minimizes Ω_s. Inserting $\overline{l}(\mathbf{r}_\parallel)$ into Ω_s renders a laterally varying equilibrium wall-vapor surface tension $\sigma_{wg}(\mathbf{r}_\parallel)$ such that

$$\int_A d^2 r_\parallel\ \sigma_{wg}(\mathbf{r}_\parallel) = \min_{\{l(\mathbf{r}_\parallel)\}} \Omega_s[l(\mathbf{r}_\parallel)] = \Omega_s[\overline{l}(\mathbf{r}_\parallel)], \tag{6.9}$$

where [see Eq. (6.3)]

$$\sigma_{wg}(\mathbf{r}_\parallel) = \Delta\Omega_b \overline{l}(\mathbf{r}_\parallel) + \sigma_{wl}(\mathbf{r}_\parallel; d_w(\mathbf{r}_\parallel)) + \Sigma_{lg}(\mathbf{r}_\parallel, [\overline{l}(\mathbf{r}_\parallel)])$$
$$+ \omega(\mathbf{r}_\parallel, \overline{l}(\mathbf{r}_\parallel); d_w(\mathbf{r}_\parallel)) + \mathcal{C}(\mathbf{r}_\parallel, \overline{l}(\mathbf{r}_\parallel); [d_w(\mathbf{r}_\parallel)]). \tag{6.10}$$

Within the local theory and for $d_w(\mathbf{r}_\parallel) \equiv d_w$, Eq. (6.10) reduces to

$$\sigma_{wg}(\mathbf{r}_\parallel) = \Delta\Omega_b \overline{l}(\mathbf{r}_\parallel) + \sigma_{wl}(\mathbf{r}_\parallel) + \sigma_{lg}\sqrt{1 + (\nabla_\parallel \overline{l}(\mathbf{r}_\parallel))^2}$$
$$+ \omega(\mathbf{r}_\parallel, \overline{l}(\mathbf{r}_\parallel)) \tag{6.11}$$

with the corresponding ELE

$$\sigma_{lg} \nabla \cdot \left(\frac{\nabla \overline{l}(\mathbf{r}_\parallel)}{\sqrt{1 + (\nabla \overline{l}(\mathbf{r}_\parallel))^2}} \right) = \Delta\Omega_b + \left. \frac{\partial \omega(\mathbf{r}_\parallel, l)}{\partial l} \right|_{l=\overline{l}(\mathbf{r}_\parallel)}$$
$$= \Delta\Omega_b - \Delta\rho\rho_l t(\overline{l}(\mathbf{r}_\parallel) - d_w)$$
$$+ \Delta\rho V(\mathbf{r}_\parallel, \overline{l}(\mathbf{r}_\parallel)). \tag{6.12}$$

This type of equation is often used (e.g., in Ref. [32]) to study the macroscopic properties of liquidlike wetting layers and droplets on structured substrates. This section provides a microscopic basis for the underlying concept of a local, spatially varying surface tension as it is used in several studies (e.g., in Refs. [31–33]).

VII. SUMMARY

We have obtained the following main results.

(1) Based on the description of wetting phenomena on homogeneous substrates within the framework of density functional theory (Sec. II, Fig. 1), we have derived a systematic decomposition of the grand canonical potential of a fluid in contact with a chemically heterogeneous substrate into bulk, surface, and line contributions. The minimum of the latter yields the equilibrium morphology of the adsorbed liquidlike wetting films and the associated line tension within mean field theory. As paradigmatic cases we have studied a simple chemical step (SCS; see Fig. 2 for $n \to \infty$, and Sec. III A), a chemical step within a surface layer supported by a homogeneous substrate (LCS; see Fig. 2 and Sec. III B), and a chemical stripe (CST; see Fig. 3 and Sec. III C).

(2) Across a SCS the profiles of the liquid-vapor interface of the liquidlike adsorbed wetting film morphology interpolate between their asymptotic values corresponding to the wetting film thicknesses on the two individual, homogeneous substrates forming the SCS (Figs. 7 and 9). The curvature of the profiles changes sign near the position of the step (Fig. 4). On each side of the step the lateral width $\Delta_\pm$ of this transition region is governed by the corresponding lateral correlation length $\xi_\parallel$ of the height-height correlation function [see Figs. 8 and 10 and Eqs. (4.15) and (4.16)]. This width diverges according to power laws which depend on whether a complete or critical wetting transition (Fig. 5) is approached. Near these transitions the dependence of the profiles on the lateral coordinate x and on $\xi_\parallel$ exhibits scaling properties [Eqs. (4.17) and (4.21)] with singular scaling functions (Fig. 6) such that at the wetting transitions the profiles diverge algebraically as function of x [see Eqs. (4.19) and (4.23) and Figs. 13 and 14]. The corresponding amplitudes as well as those for the van der Waals tails of the profiles [see Eqs. (4.8) and (4.9)] have been determined analytically. The various power laws are modified by retardation (Sec. IV E). Near first-order wetting transitions the interface profiles vary on a molecular scale (Fig. 11), and are sensitive to the details of the laterally varying substrate potential.

(3) The morphology of the wetting film across a chemical step within a surface layer (LCS) is similar to that on a SCS. The confinement of the chemical heterogeneity to a thin surface layer leads to more rapidly decaying van der Waals tails [Eqs. (4.10)–(4.12)] as compared with the SCS and modified amplitudes for the power-law divergences as function of x [see the discussion after Eq. (4.24)]. The scaling functions for the SCS and LCS are the same. The main structural features of the wetting film across a LCS are already induced by very few heterogeneous surface monolayers on the substrate (Fig. 12).

(4) If the chemical heterogeneity is confined to a stripe (CST) complete wetting of the inner region is inhibited by an incompletely wetted outer region (Fig. 15). The leakage of the liquid into the outer region is governed by $\xi_\parallel$ correspond-

ing to the latter. Thus the tight confinement of the liquid to the stripe can be accomplished by choosing an embedding outer material on which only thin wetting films can form. This confinement can be achieved even if the inner material ''prefers'' macroscopically thick wetting films. In the latter case and for wide stripes with width a the interface profile has the shape of a semiellipse [Eq. (4.25)], and the excess coverage supported by the stripe scales as $a^{3/2}$ (Fig. 18). The perturbation of the interface profile near one step by the distant step has been determined analytically [Eq. (4.26)], as has the corresponding van der Waals tails characterizing the decay into the outer region [Eqs. (4.13) and (4.14)]. Only for sufficiently wide stripes can the film thickness on the stripe attain the value l_+ for the corresponding homogeneous case (Fig. 16). If, on the other hand, the outer region undergoes a complete or critical wetting transition but the inner region does not favor it, the thickening wetting film spills over into the stripe region and drags its wetting behavior along, leaving behind a dent (Fig. 17). The depth of the dent behaves nonmonotonously as function of the undersaturation $\Delta\mu$. Ultimately, for $\Delta\mu\to 0$ the depth of the dent vanishes and its width diverges proportional to $\xi_\parallel$ so that the net depletion of the coverage caused by the stripe diverges as $(\Delta\mu)^{-4/15}$ (Fig. 17).

(5) The dependence of the line tension $\tau_{\mathrm{CST}}(a)$ associated with a chemical stripe on the stripe width a leads to a lateral force per unit length $f(a)=-\partial\tau_{\mathrm{CST}}(a)/\partial a$ [Eqs. (5.2) and (5.3)] acting on the stripe and leading to a compression or dilation which is balanced by the elastic forces of the substrate. Except for small stripe widths $a\sim\sigma_f$ the constant contribution $f_0=\sigma_{w_-g}-\sigma_{w_+g}$ is the dominating one. The excess contribution $f_{\mathrm{ex}}(a)=f(a)-f_0(a)$ decays as $f_{\mathrm{ex}}(a\to\infty)\sim a^{-3}$ (Fig. 19). Whereas for solid substrates this force has practically no effect, we expect that for liquidlike wetting films on a liquid substrate decorated with a Langmuir-Blodgett film which contains a stripe of different material the force can become important. In this case the adsorbed wetting films cause a detectable change in the stripe width depending on the compressibility of the Langmuir-Blodgett films.

(6) In Sec. VI we presented a systematic microscopic derivation of the Euler-Lagrange equation [Eq. (6.12)] for a liquidlike film adsorbed on an arbitrary chemically structured substrate (Fig. 20). This approach also provides a microscopic calculus for determining local, laterally varying wall-vapor and wall-liquid surface tensions [Eqs. (6.4) and (6.10)] required for macroscopic analyses. Lateral inhomogeneities within the repulsive part of the substrate potential modify these expressions with respect to what is expected intuitively [see Eqs. (6.7) and (6.10)].

ACKNOWLEDGMENT

We gratefully acknowledge financial support by the German Science Foundation within the special research initiative *Wetting and Structure Formation at Interfaces.*

APPENDIX A: POTENTIALS OF HETEROGENEOUS SUBSTRATES

We approximately determine the substrate potential by a pairwise summation of the interaction between a single fluid particle and all substrate particles. To this end we assume that the molecules in the substrate are located at orthorhombic lattice sites with the lattice constants g_x, g_y, and g_z in the x, y, and z directions, respectively. The leading contribution from this summation corresponds to a three-dimensional integration over the substrate volume. The discrete sum generates in addition subdominant contributions which are proportional to powers of the lattice spacings. The substrate potential can be written as a sum $V(x,z)=V_{\mathrm{att}}(x,z)+V_{\mathrm{rep}}(x,z)$ of an attractive contribution and a repulsive contribution. In the attractive contribution we take into account the two leading orders of this power series, whereas the repulsive contribution is modeled by a steplike crossover between the repulsive parts of the potentials of the corresponding homogeneous, semi-infinite substrates. This assumption is justified because the repulsive interaction decays very rapidly and is only significant for $z\lesssim 1.5\sigma_f$, where $z=0$ denotes the position of the nuclei of the top substrate layer.

The different chemical species are distinguished by $+$ and $-$, denoting the different potential coefficients. If a homogeneous substrate is covered by a heterogeneous surface layer of finite thickness we denote its constituent molecules by H. For the interparticle potential we adopt the Lennard-Jones form

$$\phi_{\pm,H}(r)=4\epsilon_{\pm,H}\left[\left(\frac{\sigma_{\pm,H}}{r}\right)^{12}-\left(\frac{\sigma_{\pm,H}}{r}\right)^{6}\right]. \tag{A1}$$

Under these conditions one finds, for a SCS, i.e., for two adjacent quarter spaces w_+ and w_- (see Fig. 2 with $n=\infty$),

$$\begin{aligned}V_{\mathrm{att}}^{\mathrm{SCS}}(x,z)=&-\frac{u_3^+ +u_3^-}{2}\frac{1}{z^3}+\frac{u_3^+ -u_3^-}{2}\left(\frac{1}{x^3}-\left(\frac{r}{xz}\right)^3+\frac{3}{2}\frac{1}{xzr}\right)\\&-\frac{u_4^+ +u_4^-}{2}\frac{1}{z^4}-\frac{u_4^+ -u_4^-}{2}\left(\frac{x}{z^4r}+\frac{1}{2}\frac{x}{z^2r^3}\right)\\&+\frac{u_{4,x}^+ -u_{4,x}^-}{2}\left(\frac{1}{x^4}-\left(\frac{z}{x^4r}+\frac{1}{2}\frac{z}{x^2r^3}\right)\right)\\&+O(x^{-m}z^{-n},m+n=5),\end{aligned} \tag{A2}$$

with $r=\sqrt{x^2+z^2}$ and

$$V_{\mathrm{rep}}^{\mathrm{SCS}}(x,z)=\Theta(-x)\frac{u_9^-}{z^9}+\Theta(x)\frac{u_9^+}{z^9}. \tag{A3}$$

The coefficients $u_3^\pm$, $u_4^\pm$, and $u_9^\pm$ are defined by the potentials of the respective homogeneous, flat, semi-infinite substrates w_+ and w_- [see Eq. (2.12)], whereas $u_{4,x}^\pm=u_4^\pm g_x^\pm/g_z^\pm$.

Similarly, for the homogeneous, flat substrate w_H covered by two different, adjacent surface layers $w_{S,\pm}$ which consist of $n=d+1$ monolayers (compare Fig. 2), we obtain

$$V_{\mathrm{att}}^{\mathrm{LCS}}(x,z)=-\frac{u_3^H}{(z+(d+1)g_z)^3}-\frac{u_4^H}{(z+(d+1)g_z)^4}-\frac{u_3^++u_3^-}{2}\left(\frac{1}{z^3}-\frac{1}{(z+dg_z)^3}\right)$$
$$-\frac{u_4^++u_4^-}{2}\left(\frac{1}{z^4}+\frac{1}{(z+dg_z)^4}\right)+\frac{u_3^+-u_3^-}{2}\left[\frac{2x^4+x^2\tilde{z}^{\,2}+2\tilde{z}^4}{2x^3\tilde{z}^{\,3}\tilde{r}}-\frac{2x^4+x^2z^2+2z^4}{2x^3z^3r}\right]$$
$$-\frac{u_4^+-u_4^-}{2}\left[\frac{x(3\tilde{z}^{\,2}+2x^2)}{2\tilde{z}^{\,4}\tilde{r}^{\,3}}+\frac{x(3z^2+2x^2)}{2z^4r^3}\right]+\frac{u_{4,x}^+-u_{4,x}^-}{2}\left[\frac{\tilde{z}(3x^2+2\tilde{z}^{\,2})}{2x^4\tilde{r}^{\,3}}-\frac{z(3x^2+2z^2)}{2x^4r^3}\right]$$
$$+O(x^{-m}z^{-n},m+n=5), \tag{A4}$$

where $\tilde{z}=(z+dg_z)$, $r=\sqrt{x^2+z^2}$, $\tilde{r}=\sqrt{x^2+\tilde{z}^{\,2}}$, and

$$V_{\mathrm{rep}}^{\mathrm{LCS}}(x,z)\equiv V_{\mathrm{rep}}^{\mathrm{LCS}}(z)=\frac{u_9^H}{z^9}. \tag{A5}$$

The coefficients $u_j^{\pm}$ and u_j^H correspond to the coefficients of the homogeneous, flat substrate covered by a homogeneous surface layer [see Eqs. (2.10) and (2.11)], whereas $u_{4,x}^{H,\pm}=u_4^{H,\pm}g_x/g_z$.

Finally, for the slab w_{st} immersed in a homogeneous substrate w (see Fig. 3) the summation yields

$$V_{\mathrm{att}}^{\mathrm{CST}}(x,z)=-\frac{u_3^-}{z^3}-\frac{u_4^-}{z^4}-\frac{u_3^+-u_3^-}{2}\left(\frac{1}{X^3}-\frac{1}{Y^3}\right)-\frac{u_{4,x}^+-u_{4,x}^-}{2}\left(\frac{1}{X^4}+\frac{1}{Y^4}\right)$$
$$+\frac{u_3^+-u_3^-}{4}\left[\frac{2X^4+X^2z^2+2z^4}{z^3X^3(X^2+z^2)^{1/2}}-\frac{2Y^4+Y^2z^2+2z^4}{z^3Y^3(Y^2+z^2)^{1/2}}\right]+\frac{u_4^+-u_4^-}{4}\left[\frac{X(3z^2+2X^2)}{z^4(X^2+z^2)^{3/2}}-\frac{Y(3z^2+2Y^2)}{z^4(Y^2+z^2)^{3/2}}\right]$$
$$+\frac{u_{4,x}^+-u_{4,x}^-}{4}\left[\frac{z(3X^2+2z^2)}{X^4(X^2+z^2)^{3/2}}+\frac{z(3Y^2+2z^2)}{Y^4(Y^2+z^2)^{3/2}}\right]+O(x^{-m}z^{-n},m+n=5), \tag{A6}$$

where the abbreviations X and Y denote $X=x-a/2$ and $Y=x+a/2$, and

$$V_{\mathrm{rep}}^{\mathrm{CST}}(x,z)=\Theta\left(|x|-\frac{a}{2}\right)\frac{u_9^-}{z^9}+\Theta\left(\frac{a}{2}-|x|\right)\frac{u_9^+}{z^9}, \tag{A7}$$

with the coefficients defined as above for the SCS.

At large separations between a fluid particle and the substrate retardation effects set in, so that $\phi_{\pm,\mathrm{att}}(r\to\infty)\sim r^{-7}$ [48]. In this case the leading contribution to $V_{\mathrm{att}}^{\mathrm{SCS}}(x,z)$ is

$$V_{\mathrm{att}}(x,z)=-\frac{v_4^++v_4^-}{2z^4}+\frac{v_4^+-v_4^-}{2}\left\{\frac{1}{x^4}-\frac{2}{\pi}\left(\frac{\arctan(x/z)}{z^4}+\frac{\arctan(z/x)}{x^4}\right)+\frac{2}{3\pi}\frac{x^2-3z^2}{z^3x^3}-\frac{8}{3\pi}\frac{x}{z^3(x^2+z^2)}\right\}$$
$$+O(x^{-m}z^{-n},m+n=5). \tag{A8}$$

APPENDIX B: DECOMPOSITION OF THE GRAND CANONICAL DENSITY FUNCTIONAL

1. Single chemical step

The sharp-kink ansatz [Eq. (3.3)] for Eq. (2.1) leads to the decomposition of the grand canonical free energy given by Eqs. (3.4), (2.7), and (3.5), with

$$\Omega_s^{\pm}(l_{\pm})=l_{\pm}\Delta\Omega_b+\sigma_{w_{\pm}l}+\sigma_{lg}+\omega(l_{\pm}), \tag{B1}$$

where the effective interface potentials $\omega_{\pm}(l)$ are given by [compare with Eq. (2.19)]

$$\omega_{\pm}(l)=\Delta\rho\left\{\rho_l\int_{l-d_w^{\pm}}^{\infty}dz\ t(z)-\int_l^{\infty}dz\ V_{\pm}(z)\right\}. \tag{B2}$$

Here we have omitted artificial contributions generated by truncating the system; these contributions are discussed in Ref. [51]. The surface contribution is that of two half substrates w_+ and w_- covered by liquidlike wetting layers of

thickness l_+ and l_-, which are exposed to the potentials $V_+(z)$ and $V_-(z)$, respectively, of the corresponding semi-infinite, homogeneous substrates. This defines a reference system such that the deviation of the smooth profile $l(x)$ from the reference configuration (see the dashed lines in Figs. 2 and 3), due to the heterogeneity and to the smooth crossover of $V(x,z)$ from $V_-(z)$ to $V_+(z)$, leads to the line contribution

$$\Omega_l[l(x)]=\tau(d_w^{\pm},l_{\pm})+\tilde{\omega}[l(x)]. \tag{B3}$$

The term $\tau(d_w^{\pm},l_{\pm})$, which is independent of $l(x)$, is given in Eqs. (B12), (B19), and (B20) in Ref. [51]. [We note that there the plus sign of the last term in Eq. (B20) must be replaced by a minus sign.] The contribution which depends functionally on $l(x)$ reads

$$\begin{aligned}\tilde{\omega}[l(x)]=&\Delta\Omega_b\Gamma_{\rm ex}+\int_{-\infty}^{\infty}dx\{\omega(x,l(x);d_w^+)\\&-\omega(x,l_\infty(x);d_w^+)\}\\&-\Delta\rho\rho_l\left(\int_{-\infty}^{\infty}dx\int_{l(x)-d_w^+}^{l_\infty(x)-d_w^+}dz\ \overline{t}(x,z)\right.\\&\left.-\int_{-\infty}^{\infty}dx\int_{l(x)-d_w^-}^{l_\infty(x)-d_w^-}dz\ \overline{t}(x,z)\right)\\&-\frac{1}{2}(\Delta\rho)^2\int_{-\infty}^{\infty}dx\int_{-\infty}^{\infty}dx'\int_0^{\infty}dz\\&\times\int_0^{l(x)-l(x')}dz'\ \overline{w}(x-x',z-z'),\end{aligned} \tag{B4}$$

where $l_\infty(x)=l_-\Theta(-x)+l_+\Theta(x)$. The first term measures the cost in free energy for replacing a certain volume of vapor by the liquid phase. It is proportional to the excess coverage

$$\Gamma_{\rm ex}=\int_{-\infty}^{\infty}dx[l(x)-l_\infty(x)], \tag{B5}$$

and vanishes at coexistence $\mu=\mu_0$. The second term is the integrated ''local'' effective interface potential

$$\omega(x,l;d_w)=\Delta\rho\left\{\rho_l\int_{l-d_w}^{\infty}dz\ t(z)-\int_l^{\infty}dz\ V(x,z)\right\}. \tag{B6}$$

The third term, involving integrals of

$$\overline{t}(x,z)=\int_x^{\infty}dx'\int_z^{\infty}dz'\ \overline{w}(x',z'), \tag{B7}$$

takes into account the difference between d_w^- and d_w^+ and vanishes for $d_w^-=d_w^+$. The last contribution, with

$$\overline{w}(x,z)=\int_{-\infty}^{\infty}dy\tilde{w}(\sqrt{x^2+y^2+z^2}), \tag{B8}$$

describes the free energy of the deformed free liquid-vapor interface. It is a *nonlocal* functional of $l(x)$. A gradient expansion to the first order of this contribution yields the fourth term of the corresponding *local* functional $\tilde{\omega}_{\rm loc}[l(x)]$:

$$\begin{aligned}&-\frac{1}{2}(\Delta\rho)^2\int_{-\infty}^{\infty}dx\int_{-\infty}^{\infty}dx'\int_0^{\infty}dz\\&\quad\times\int_0^{l(x)-l(x')}dz'\,\overline{w}(|x-x'|,|z-z'|)\\&\quad\to\sigma_{lg}\int_{-\infty}^{\infty}dx\left\{\sqrt{1+\left(\frac{dl}{dx}\right)^2}-1\right\}.\end{aligned} \tag{B9}$$

2. Chemical stripe

The sharp-kink approximation of the density profile for the CST is

$$\begin{aligned}\hat{\rho}(x,z)=&\left\{\Theta\left(|x|-\frac{a}{2}\right)\Theta(z-d_w^-)+\Theta\left(\frac{a}{2}-|x|\right)\Theta(z-d_w^+)\right\}\\&\times[\Theta(l(x)-z)\rho_l+\Theta(z-l(x))\rho_g].\end{aligned} \tag{B10}$$

Insertion of $\hat{\rho}(x,z)$ into Eq. (2.1) leads to the decomposition

$$\begin{aligned}&\Omega([\hat{\rho}(x,z)];T,\mu;[\tilde{w}],[V])\\&\quad=\Lambda\Omega_b(\rho_g,T,\mu)+A\Omega_s(l_-;T,\mu;[\tilde{w}],[V])\\&\qquad+L_y\Omega_l([l(x)];T,\mu;[\tilde{w}],[V]),\end{aligned} \tag{B11}$$

with Ω_b given by Eq. (2.7). The surface contribution stems from the reference system which in the case of the CST is the structured substrate covered by a liquidlike layer of thickness l_- that is exposed to the potential $V_-(z)$,

$$\Omega_s(l_-)=\Omega_s^-(l_-), \tag{B12}$$

with $\Omega_s^-(l_-)$ defined by Eqs. (B1) and (B2).

The line contribution for the CST is given by

$$\Omega_l[l(x)]=\tau(d_w^{\pm},l_-)+\tilde{\omega}[l(x)], \tag{B13}$$

and represents the free energy associated with the deviation of $l(x)$ from the asymptotic value l_-, i.e., of the reference configuration. In Eq. (B13) the first term does not depend on $l(x)$:

$$\tau(d_w^{\pm},l_-)=-a(d_w^+-d_w^-)\Omega_b^{(l)}-(d_w^+-d_w^-)\rho_l^2\int_0^\infty dz\ t(z)-a\rho_l\int_{d_w^-}^{d_w^+}dz\ V_-(z)$$
$$+2\rho_l^2\left\{\int_0^\infty dx\int_0^\infty dz-\int_0^\infty dx\int_{d_w^+-d_w^-}^\infty dz-\int_a^\infty dx\int_0^\infty dz+\int_a^\infty dx\int_{d_w^+-d_w^-}^\infty dz\right\}\overline{t}(x,z)$$
$$+\rho_l\int_{-\infty}^\infty dx\int_{d_w^\infty(x)}^\infty dz\ \delta V(x,z)-\Delta\rho\int_{-\infty}^\infty dx\int_{l_-}^\infty dz\ \delta V(x,z), \tag{B14}$$

with $\delta V(x,z)=V(x,z)-V_-(z)$ and $d_w^\infty(x)=\Theta(|x|-a/2)d_w^-+\Theta(a/2-|x|)d_w^+$. The interpretation of the different terms in Eq. (B14) is analogous to the SCS (compare Ref. [51]). The second term in Eq. (B13) depends on $l(x)$

$$\tilde{\omega}[l(x)]=\Delta\Omega_b\Gamma_{\rm ex}^{\rm CST}+\int_{-\infty}^\infty dx\{\omega(x,l(x);d_w^-)-\omega(x,l_-;d_w^-)\}$$
$$+\Delta\rho\rho_l\int_{-\infty}^\infty dx\int_{-a/2}^{a/2}dx'\int_{l(x)-d_w^+}^{l(x)-d_w^-}dz\int_z^\infty dv\ \overline{w}(x-x',v)$$
$$-\frac{1}{2}(\Delta\rho)^2\int_{-\infty}^\infty dx\int_{-\infty}^\infty dx'\int_0^\infty dz\int_0^{l(x)-l(x')}dz'\ \overline{w}(x-x',z-z'), \tag{B15}$$

with

$$\Gamma_{\rm ex}^{\rm CST}=\int_{-\infty}^\infty dx[l(x)-l_-]. \tag{B16}$$

The interpretation of the first two terms is the same as for the SCS; the third term is generated by the difference of the excluded volumes at the surfaces of the inner and outer regions, and vanishes if $d_w^+=d_w^-$. The last term is the same as in Eq. (B4).

The corresponding local functional expression $\tilde{\omega}_{\rm loc}[l(x)]$ follows by replacing the last term in Eq. (B15) by the local functional given in Eq. (B9). We note that for all three substrate types (SCS, LCS, and CST) the functionals $\tilde{\omega}[l(x)]$ (and therefore also $\tilde{\omega}_{\rm loc}[l(x)]$) exhibit the same structure if $d_w^+=d_w^-$.

[1] W. Hansen, J. P. Kotthaus, and U. Merkt, in *Nanostructured Systems*, edited by M. Reed, Semiconductors and Semimetals Vol. 35 (Academic, London, 1992), p. 279; P. Bönsch, D. Wüllner, T. Schrimpf, A. Schlachetzki, and R. Lacmann, J. Electrochem. Soc. **145**, 1273 (1998); J. Wang, D.A. Thompson, and J.G. Simmons, *ibid.* **145**, 2931 (1998).

[2] D.W.L. Tolfree, Rep. Prog. Phys. **61**, 313 (1998).

[3] Y. Xia and G.M. Whitesides, Annu. Rev. Mater. Sci. **28**, 153 (1998).

[4] F. Burmeister, C. Schäfle, B. Keilhofer, C. Bechinger, J. Boneberg, and P. Leiderer, Adv. Mater. **10**, 495 (1998).

[5] J.A. Rogers, Z. Bao, and L. Dhar, Appl. Phys. Lett. **73**, 294 (1998).

[6] J. Aizenberg, A.J. Black, and G.M. Whitesides, Nature (London) **394**, 868 (1998).

[7] S. Dietrich, in *Fluids in Contact with Structured Substrates*, Vol. 529 of *NATO Advanced Study Institute, Series C*: *New Approaches to Problems in Liquid State Theory*, edited by C. Caccamo, J.P. Hansen, and G. Stell (Kluwer, Dordrecht, 1999), p. 197.

[8] A. Paterson and M. Fermigier, Phys. Fluids **9**, 2210 (1997).

[9] G. Wiegand, T. Jaworek, G. Wegner, and E. Sackmann, J. Colloid Interface Sci. **196**, 299 (1997).

[10] P. Zeppenfeld, V. Diercks, C. Tölkes, R. David, and M.A. Krzyzowski, Appl. Surf. Sci. **130-132**, 484 (1998).

[11] A. Karim, J.F. Douglas, B.P. Lee, S.C. Glotzer, J.A. Rogers, R.J. Jackman, E.J. Amis, and G.M. Whitesides, Phys. Rev. E **57**, R6273 (1998).

[12] T. Pompe, A. Fery, and S. Herminghaus, Langmuir **14**, 2585 (1998).

[13] L. Rockford, Y. Liu, P. Mansky, T.P. Russell, M. Yoon, and S.G.J. Mochrie, Phys. Rev. Lett. **82**, 2602 (1999).

[14] H. Gau, S. Herminghaus, P. Lenz, and R. Lipowsky, Science **283**, 46 (1999).

[15] B.S. Gallardo, V.K. Gupta, F.D. Eagerton, L.I. Jong, V.S. Craig, R.R. Shah, and N.L. Abbott, Science **283**, 57 (1999).

[16] C.S. Chen, M. Mrksich, S. Huang, G.M. Whitesides, and D.E. Ingber, Science **276**, 1425 (1997).

[17] M. Matsuzawa, K. Kobayashi, K. Sugioka, and W. Knoll, J. Colloid Interface Sci. **202**, 213 (1998).

[18] E. Delamarche, A. Bernard, H. Schmidt, B. Michel, and H.A. Biebuyck, Science **276**, 779 (1997).

[19] H. Shi, W.-B. Tsai, M.D. Garrison, S. Ferrari, and B.D. Ratner, Nature (London) **398**, 593 (1999).

[20] J.B. Knight, A. Vishwanath, J.P. Brody, and R.H. Austin, Phys. Rev. Lett. **80**, 3863 (1998).

[21] M. Grunze, Science **283**, 41 (1999).
[22] R.F. Service, Science **282**, 399 (1998).
[23] J.L. Wilbur, A. Kumar, E. Kim, and G.M. Whitesides, Adv. Mater. **6**, 600 (1994).
[24] A. Kumar, H.A. Biebuyck, and G.M. Whitesides, Langmuir **10**, 1498 (1994).
[25] R.J. Jackman, J.L. Wilbur, and G.M. Whitesides, Science **269**, 664 (1995).
[26] P.C. Hidber, W. Helbig, E. Kim, and G.M. Whitesides, Langmuir **12**, 1375 (1996).
[27] J.R. Henderson, J. Phys.: Condens. Matter **11**, 629 (1999).
[28] Y. Pomeau and J. Vannimenus, J. Colloid Interface Sci. **104**, 477 (1985).
[29] M.O. Robbins, D. Andelman, and J.-F. Joanny, Phys. Rev. A **43**, 4344 (1991).
[30] C.J. Boulter, Phys. Rev. E **57**, 2062 (1998).
[31] P. Lenz and R. Lipowsky, Phys. Rev. Lett. **80**, 1920 (1998).
[32] P.S. Swain and R. Lipowsky, Langmuir **14**, 6772 (1998).
[33] R. Lipowsky, P. Lenz, and P. S. Swain, Colloids Surf., A (to be published).
[34] C. Bauer, S. Dietrich, and A.O. Parry, Europhys. Lett **47**, 474 (1999).
[35] S. Nechaev and Y.-C. Zhang, Phys. Rev. Lett. **74**, 1815 (1995).
[36] D. Urban, K. Topolski, and J. De Coninck, Phys. Rev. Lett. **76**, 4388 (1996).
[37] T.W. Burkhardt, J. Phys. A **31**, L549 (1998).
[38] M.W. Cole and E. Vittoratos, J. Low Temp. Phys. **22**, 223 (1976).
[39] L. Łajtar and S. Sokołowski, J. Chem. Soc., Faraday Trans. **88**, 2545 (1992).
[40] C. Chmiel, K. Karykowski, A. Patrykiejew, W. Rżysko, and S. Sokołowski, Mol. Phys. **81**, 694 (1994).
[41] P. Röcken, A. Somoza, P. Tarazona, and G. Findenegg, J. Chem. Phys. **108**, 8689 (1998).
[42] L.J. Douglas Frink and A.G. Salinger, J. Chem. Phys. **110**, 5969 (1999).
[43] S.K. Nath, P.F. Nealey, and J.J. de Pablo, J. Chem. Phys. **110**, 7483 (1999).
[44] W. Gac, A. Patrykiejew, and S. Sokołowski, Surf. Sci. **306**, 434 (1994); Thin Solid Films **298**, 22 (1997).
[45] M. Schoen and D.J. Diestler, Chem. Phys. Lett. **270**, 339 (1997); Phys. Rev. E **56**, 4427 (1997).
[46] H. Bock and M. Schoen, Phys. Rev. E **59**, 4122 (1999).
[47] S. Curtarolo, M.W. Cole, M.J. Bojan, and W.A. Steele, Phys. Rev. E **59**, 4402 (1999).
[48] J. Israelachvili, *Intermolecular and Surface Forces*, 2nd ed. (Academic, London, 1991).
[49] S. Dietrich and M. Schick, Phys. Rev. B **33**, 4952 (1986).
[50] S. Dietrich, in *Phase Transitions and Critical Phenomena*, edited by C. Domb and J.L. Lebowitz (Academic, London, 1988), Vol. 12, p. 1.
[51] W. Koch, S. Dietrich, and M. Napiórkowski, Phys. Rev. E **51**, 3300 (1995).
[52] R. Evans, Adv. Phys. **28**, 143 (1979).
[53] J.D. Weeks, D. Chandler, and H.C. Andersen, J. Chem. Phys. **54**, 5237 (1971); H.C. Andersen, J.D. Weeks, and D. Chandler, Phys. Rev. A **4**, 1597 (1971).
[54] N.F. Carnahan and K.E. Starling, J. Chem. Phys. **51**, 635 (1969).
[55] P.G. de Gennes, Rev. Mod. Phys. **57**, 827 (1985).
[56] M. Schick, in *Liquids at Interfaces*, Proceedings of the Les Houches Summer School Lectures, Session XLVIII, edited by J. Chavrolin, J. F. Joanny, and J. Zinn-Justin (Elsevier, Amsterdam, 1990), p. 415.
[57] D.E. Sullivan and M.M. Telo da Gama, in *Fluid Interfacial Phenomena*, edited by C. A. Croxton (Wiley, New York, 1986), p. 45.
[58] R. Evans, in *Fundamentals of Inhomogeneous Fluids*, edited by D. Henderson (Dekker, New York, 1992), p. 85; see Sec. V therein.
[59] M. Napiórkowski and S. Dietrich, Phys. Rev. B **34**, 6469 (1986); Europhys. Lett. **9**, 361 (1989); S. Dietrich and M. Napiórkowski, Phys. Rev. A **43**, 1861 (1991).
[60] S. Dietrich, in *Phase Transitions in Surface Films 2*, Vol. 267 of *NATO Advanced Study Institute, Series B: Physics*, edited by H. Taub, G. Torzo, and H.J. Lauter (Kluwer, Dordrecht), 1991, p. 391.
[61] M. Kagan, W.V. Pinczewski, and P.E. Oren, J. Colloid Interface Sci. **170**, 426 (1995).
[62] C. Bauer and S. Dietrich, Eur. Phys. J. B **10**, 767 (1999).
[63] R. Lipowsky, Phys. Rev. B **32**, 1731 (1985).
[64] M.P. Nightingale, W.F. Saam, and M. Schick, Phys. Rev. B **30**, 3830 (1984).
[65] E. Cheng, M.W. Cole, J. Dupont-Roc, W.F. Saam, and J. Treiner, Rev. Mod. Phys. **65**, 557 (1993).
[66] R. Hallock, J. Low Temp. Phys. **101**, 31 (1995), and references therein.
[67] K. Ragil, J. Meunier, D. Broseta, J.O. Indekeu, and D. Bonn, Phys. Rev. Lett. **77**, 1532 (1996); N. Shahidzadeh, D. Bonn, K. Ragil, D. Broseta, and J. Meunier, *ibid.* **80**, 3992 (1998).
[68] T. Pfohl and H. Riegler, Phys. Rev. Lett. **82**, 783 (1999).
[69] D. Beysens, in *Liquids at Interfaces* (Ref. [56]), p. 499.
[70] H.I. Kim, C.M. Mate, K.A. Hannibal, and S.S. Perry, Phys. Rev. Lett. **82**, 3496 (1999).
[71] S. Herminghaus, K. Jacobs, K. Mecke, J. Bischof, A. Fery, M. Ibn-Elhaj, and S. Schlagowski, Science **282**, 916 (1998).
[72] M.E. Fisher and A.J. Jin, Phys. Rev. B **44**, 1430 (1991); Phys. Rev. Lett. **69**, 792 (1992).
[73] A.O. Parry and R. Evans, Mol. Phys. **78**, 1527 (1993).